https://doi.org/10.5194/egusphere-2026-5308
Preprint. Discussion started: 11 September 2026

Seasonal divergence in phytoplankton community and size structure in contrasting fjord types in SW Greenland

Marta Mikhno[1], Lorenz Meire[2,3], Renaat Dasseville[1], Peter Chaerle[1], Ilse Daveloose[1], Sofie D'hondt[1], Koen Sabbe[1]

[1] Laboratory of Protistology and Aquatic Ecology, Department of Biology, Ghent University, Ghent, 9000, Belgium
[2] Department of Estuarine and Delta Systems, Royal Netherlands Institute for Sea Research, Yerseke, 4400, Netherlands
[3] Greenland Climate Research Centre, Greenland Institute of Natural Resources, Nuuk, 3900, Greenland

Correspondence to: Koen Sabbe (koen.sabbe@ugent.be)

Abstract

Arctic fjords are coastal ecosystems whose productivity is strongly impacted by glacial meltwater. Fjords affected by marine-terminating glaciers (MTGs) sustain highly productive, diatom-dominated blooms throughout the growing season, whereas fjords with land-terminating glaciers (LTGs) typically experience a diatom spring bloom followed by less productive, small-celled communities in summer. However, the biomass, community composition and size structure of these phytoplankton communities, particularly pico- and nano-sized components, remain underexplored. We investigated spring–summer contrasts in the phytoplankton of two adjacent SW Greenland fjords: Nuup Kangerlua, mainly impacted by MTGs, and Ameralik, impacted only by an LTG. Combining high-throughput imaging, pigment and metabarcoding approaches allowed us to resolve the functional (size, pigmentation) and taxonomic composition of the phytoplankton communities. Our analyses revealed seasonal divergence between the two fjords. In spring, both were dominated by colony-forming diatoms under nutrient-replete conditions. In summer, nanophytoplankton dominated both fjords. However, persistent subglacial upwelling sustained growth of non-colonial diatoms in the MTG fjord, whereas pico- and nano-sized chlorophytes and cryptophytes dominated the warmer, less saline, turbid and highly stratified surface waters of the LTG fjord. Increased importance of mixotrophy under these conditions suggests an efficient microbial loop, partly relying on regenerated nitrogen. In contrast, the inner MTG fjord was characterized by the harmful haptophyte *Pseudohaptolina birgeri*. Despite these compositional differences, phytoplankton biomass and primary production remained similar between fjords. Overall, our results suggest that continued glacial melt and retreat of MTGs onto land will alter phytoplankton community organization, with cascading effects on Arctic food webs and carbon cycling.

1 Introduction

Greenland's fjords are among the most productive Arctic ecosystems, acting as critical carbon sinks (Meire et al., 2015; Rysgaard et al., 2012) and supporting valuable fisheries (Meire et al., 2017). Their productivity is closely tied to the type and magnitude of glacial influence. Marine-terminating glaciers (MTGs), or tidewater outlet glaciers, release subglacial meltwater that causes plume-driven upwelling of nutrient-rich deep waters, stimulating primary production in surface waters throughout the growing season (Cape et al., 2019; Hopwood et al., 2018; Meire et al., 2017). In contrast, riverine runoff from land-terminating glaciers (LTGs) enhances stratification and turbidity in surface waters. This reduces vertical mixing and limits light and nutrient availability, leading to

https://doi.org/10.5194/egusphere-2026-5308
Preprint. Discussion started: 11 September 2026

reduced productivity in summer (Hopwood et al., 2020; Meire et al., 2017). As the Greenland Ice Sheet (GrIS) retreats in response to climate warming (King et al., 2018; The IMBIE Team, 2020; Van Den Broeke et al., 2016), MTGs are transitioning into LTGs. This shift is expected to fundamentally alter fjord hydrography and nutrient supply, raising concerns about long-term ecological and socio-economic impacts on these ecosystems (Carr et al., 2017; Meire et al., 2017).

Phytoplankton plays a pivotal role in primary production, nutrient regeneration, and carbon transfer in fjord food webs (Han et al., 2024; Juul-Pedersen et al., 2015). It encompasses a wide range of sizes, metabolic strategies and nutrient requirements, and can rapidly respond to environmental change (Falkowski et al., 2004), including glacial influence (Hernando et al., 2020; White et al., 2025). In Arctic fjords, MTG fjords commonly sustain productive diatom blooms from spring to summer because of subglacial discharge-driven nutrient resupply throughout the growing season. In contrast, in LTG fjords, the absence of subglacial discharge drives a shift from the diatom spring bloom to pico- and nanoplankton-dominated communities in summer (Dąbrowska et al., 2025; Kanna et al., 2022; Meire et al., 2023; Stuart-Lee et al., 2023). A transition from MTG to LTG conditions is therefore expected not only to reduce annual primary productivity but also to reorganize phytoplankton taxonomic and size structure and trophic transfer (Meire et al., 2023). This has been demonstrated in the SW Greenland fjords Nuup Kangerlua and Ameralik, where recent studies have linked contrasting glacial regimes to differences in ecosystem structure and seasonal bloom dynamics. Meire et al. (2023) showed that the LTG-fjord Ameralik had lower annual primary production and CO_2 uptake, with a greater importance of microbial recycling pathways and smaller planktonic size classes, than MTG-dominated Nuup Kangerlua. Stuart-Lee et al. (2023) further showed that Nuup Kangerlua can sustain diatom blooms throughout summer, whereas Ameralik tends to shift toward pico- and nanoplankton-dominated communities.

Despite growing evidence for glacial control on fjord microbial communities, seasonal differences in phytoplankton taxonomic and functional community structure remain poorly resolved, especially for the nano- and pico-sized components. This is partly related to the use of different methods which capture different facets of community structure (composition, size, pigmentation) at different levels of taxonomic resolution. The aim of this study is to perform an in-depth analysis of seasonal differences (spring vs. summer) in phytoplankton communities in two fjord systems in SW Greenland, viz. MTG-dominated Nuup Kangerlua (hereafter referred to as the MTG-fjord) and LTG-impacted Ameralik (hereafter referred to as the LTG-fjord). Combining high-throughput imaging (imaging flow cytometry and FlowCAM), biochemical (pigments) and molecular (18S rRNA gene amplicon sequencing) approaches allowed obtaining a highly resolved overview of the biomass and taxonomic and functional (size, pigments) of the phytoplankton. We then assessed how variation in biomass and structure were related to primary production and potential environmental drivers, such as turbidity, nutrient availability, and water column stratification.

On the basis of existing literature, we hypothesized that: (i) spring phytoplankton communities were similar in both fjords types, reflecting synchronized bloom dynamics under nutrient replete conditions; (ii) in summer, contrasting glacial impacts would drive divergence in community structure, with a shift to smaller (pico- and nano-sized) phototrophs in the LTG fjord, while sustaining diatom production in the MTG-fjord; (iii) summer communities exhibited a greater reliance on alternative trophic strategies (e.g. mixotrophy) in response to nutrient depletion, particularly in the stratified surface waters of the LTG fjord, favouring small flagellates.

https://doi.org/10.5194/egusphere-2026-5308
Preprint. Discussion started: 11 September 2026

2 Material and Methods

2.1 Study area and sampling strategy

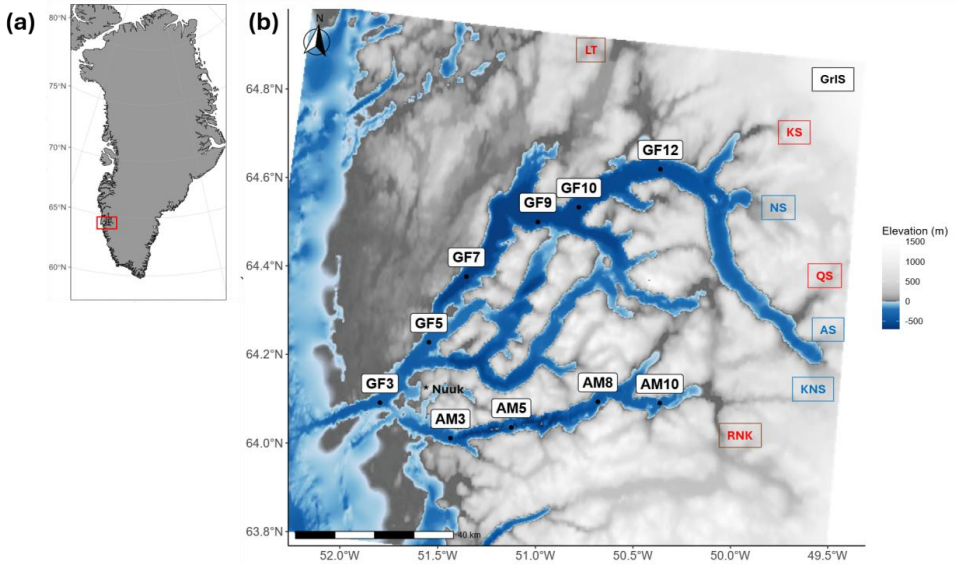

Figure 1: *Map of the study area. (a) Location of NK and AM fjords in SW Greenland. (b) Detailed view of the fjords showing sampling stations (black dots) labeled as GFx in NK and AMx in AM. Acronyms indicate freshwater sources: the Greenland Ice Sheet (GrIS); marine-terminating glaciers (MTG, blue): Kangiata Nunaata Sermia (KNS), Akugdlersuup Sermia (AS), and Narsap Sermia (NS); land-terminating glaciers (LTG) and associated freshwater bodies (red): Qamanaarssuup Sermia (QS), Kangilinguata Sermia (KS), River Naajat Kuuat (RNK), and Lake Tasersuaq (LT). Bathymetric data: GEBCO Compilation Group (2024), GEBCO 2024 Grid (doi:10.5285/1c44ce99-0a0d-5f4f-e063-7086abc0ea0f).*

Nuup Kangerlua (NK) is a large fjord system located in SW Greenland (64°10′N,51°44′W) (Fig. 1). Covering an area of 2,013 km², the fjord has an average depth of ~250 meters, with its deepest point >600 m (Mortensen et al., 2011). The system is divided into multiple branches, with the main branch ~190 km long. The fjord features several sills, the most prominent of which is located at its entrance at a depth of ~170 m (Mortensen et al., 2011). The inner part of the fjord is directly connected to three MTGs from the GrIS and three LTGs (Fig. 1b). Ameralik (AM) is located just south of NK, with an area of 400 km² and a length of ~75 km (Fig. 1). At its entrance, a 110 m deep sill restricts deep water exchange, while the central part of the fjord features a series of deep basins, reaching a maximum depth of ± 700 m (Stuart-Lee et al., 2021). AM is fed by LTGs only, with glacial meltwater primarily delivered via the river Naajat Kuuat. In each fjord system, 5 summer and 6 spring stations in NK (GFx), and 4 (summer and spring) stations in AM (AMx) were sampled aboard RV *Avataq* in August 2021 and May 2022. Unless specified otherwise, water samples were collected using a 5 L Niskin bottle at discrete depths: 1 m (surface); 5 and 10 m (sub-surface); 20 and 40 m (below the deep chlorophyll maximum, bDCM); and 150 and 300 m (deep), as well as at the deep chlorophyll maximum (DCM), which was identified on board from fluorometric profiles (see below). A table summarizing sampling locations, dates, and DCM depths is provided in the Supplementary (Tab. S1).

https://doi.org/10.5194/egusphere-2026-5308
Preprint. Discussion started: 11 September 2026

2.2 Environmental data and primary production

Vertical profiles of water temperature, salinity, density anomaly, turbidity, photosynthetically active radiation (PAR), and fluorescence were obtained using a CTD profiler (SBE 19plus) equipped with a Seapoint Chlorophyll Fluorometer and a Biospherical/Licor quantum Q PAR sensor. Measurements were recorded from the surface down to approximately 5 m above the seafloor. Chl a depth profiles were constructed using the fluorescence data. As fluorescence per unit of Chl a varied systematically with depth, a fluorescence-based Chl a factor (F_{chl}=F/[Chl]) was calculated by relating measured Chl a concentrations at discrete depths (see Sect. 2.4) to fluorometer measurements at the same depths. F_{chl} values between sampling depths were then assigned by linear interpolation (Lyngsgaard et al., 2014) at 1 m resolution. The resulting F_{chl} (z) profile was then used to estimate a continuous Chl a profile as Chl(z)=F(z)/ F_{chl} (z). For macronutrient analysis, 10 mL subsamples were filtered through 0.45 µm Q-Max GPF syringe filters and immediately frozen at -20°C until further analysis. Nitrate (NO_3^-), nitrite (NO_2^-), phosphate (PO_4^{+3}), silicate (SiO_2), and ammonium (NH_4^+) concentrations were determined using standard colorimetric methods with a Seal QuAAtro autoanalyzer (Graßhoff et al., 2009).

Primary production (PP) was measured using the ^{14}C incubation method (Nielsen, 1952). Seawater samples were collected at discrete depths of 1, 5, 10, 20, 40 and 50 m, and the DCM. Incubation bottles were filled with 55 mL of unfiltered seawater and spiked with 175 µL $NaH^{14}CO_3$ (20 µCi mL^{-1}), then incubated at *in situ* temperature for 2 h in an ICES incubator (Hydro-Bios, Germany). Samples were subsequently filtered onto 25 mm GF/F filters (Whatman), and 100 µL of 1 M HCl was added to remove excess $NaH^{14}CO_3$. Filters were left open for 24 h under a fume hood before adding 10 mL of scintillation cocktail (Ultima Gold, PerkinElmer) and counting radioactivity using a liquid scintillation analyzer (Tri-Carb 2800TR, PerkinElmer). After subtracting dark fixation rates, PP was calculated based on measured dissolved inorganic carbon (DIC) concentrations and reported as depth-integrated rates (0-50m).

2.3 Plankton abundance and carbon biomass

The abundance of pico-, nano- and microplankton (≤100 µm) cells was analysed using Imaging Flow Cytometry (iFCM) with an ImageStream®X Mk II. As the upper size limit of this instrument is 100 µm, 5 mL of seawater sample was filtered through a 100 µm mesh to remove larger particles. The filtrate was then fixed with 1.0 % glutaraldehyde (final concentration) and stored at 4 °C. Samples were left to sediment for at least 48 h, after which the supernatant was removed to achieve a 4x final concentration. This concentration step was necessary due to the low abundance of larger cells in the small volume analysed by the instrument. Before data acquisition, 0.5 mL of the sample was stained with 1 % (v/v) Sybr Green I (100x working solution in DMSO) and incubated in the dark at 37 °C for 20 minutes. Microscopic images (magnification: 40x, pixel size: 0.5 × 0.5 µm) and flow cytometry data, including bright field images, fluorescence at 488 nm (Sybr Green-stained DNA/RNA), and fluorescence at 642 nm (chlorophyll autofluorescence), were recorded for further analysis. Due to technical issues encountered during fieldwork, spring samples from stations AM3 and AM5 could not be included in this analysis. Using IDEAS® software v. 6.2, plankton populations were classified and quantified based on their optical and fluorescence properties. In this study, only autofluorescent ('phytoplankton') cells were considered, as the focus was on the phototrophic component of the plankton community, including potential mixotrophs. These cells were further categorized into size-based functional groups: picophytoplankton (AP; ≤2 µm), small and large nanophytoplankton (sAN: 2–5 µm; lAN: 5–20 µm), and microphytoplankton (AMicro; 20–100 µm). This microphytoplankton fraction was likely underestimated because diatom colonies (composed of cells < 100 µm)

https://doi.org/10.5194/egusphere-2026-5308
Preprint. Discussion started: 11 September 2026

were removed during the pre-filtration step; however, these colonies were subsequently quantified through complementary FlowCAM image analyses (see below).

To estimate the biovolume of each class, the two-dimensional surface area, measured using the IDEAS® imaging software, was multiplied by the average cell width. This calculation was performed under the assumption that width approximates the third spatial dimension, i.e., cell depth (Seelam et al., 2022). This approach provides a practical estimation of cell volume by avoiding the need to assign an idealized shape to each cell type. Carbon biomass was subsequently derived from biovolume using established carbon–volume relationships following Menden-Deuer and Lessard (Menden-Deuer and Lessard, 2000). For pico- and nanophytoplankton groups (AP, sAN, lAN), carbon content was estimated using the general conversion factor (Eq. 1):

$$pg\ C\ cell^{-1} = 0.216 \times volume^{0.939} \quad (1)$$

where volume is expressed in µm³. For the largest size fraction (AMicro), dominated by large diatoms, a specific conversion for diatoms was applied (Eq. 2):

$$pg\ C\ cell^{-1} = 0.288 \times volume^{0.811} \quad (2)$$

(Menden-Deuer and Lessard, 2000). Carbon values were converted from pg C cell^{-1} to carbon biomass (µg C L^{-1}) based on cell abundance.

During both season, at stations GF5, GF7, GF12, AM3, AM5, and AM10, 10 L of seawater from the DCM was filtered through an Apstein net (20 µm mesh size) and the residue reduced to a final volume of 150 mL. The samples were preserved with acid Lugol's solution (5 % final concentration) and formaldehyde (2 % final concentration), then stored at 4 °C in the dark. Subsequently, the samples were analysed in three technical replicates (15 mL each) at the Flanders Marine Institute (VLIZ, Belgium) using a FlowCAM® v. 4 imaging system (Fluid Imaging Technologies, Yarmouth, Maine, U.S.A.) and VisualSpreadsheet® software v. 4.2.52. FlowCAM integrates flow cytometry, microscopy, and image analysis technologies (Sieracki et al., 1998). A 300-µm deep flow cell with a 4x objective was used, capturing particles with an Equivalent Spherical Diameter (ESD) between 100 and 300 µm. The autoclassification tool in VisualSpreadsheet was employed to assign the images to taxa, with subsequent validation by a taxonomist. Each particle was identified to the lowest possible taxonomic level, and the composition and relative abundance per sample were calculated. Images were categorized into following groups: 'diatom colonies', the diatom genus *Rhizosolenia*, 'individual centric' and 'individual pennate' diatoms, dinoflagellates (e.g., *Protoperidinium* and *Tripos*), ciliates (Tintinnina), and zooplankton-related categories (e.g., copepods, nauplii, crustaceans, rotifers, and ascidian larvae). Non-living material (e.g., detritus, fecal pellets, fibers) was grouped as detrital matter, and unclassified particles were considered as a separate category. Additionally, images of the 'diatom colonies' group were analyzed using ImageJ software (Schneider et al., 2012) combined with a custom image processing algorithm. From these analyses, the absolute cell concentration, total surface area, and cell size were quantified. Carbon biomass estimates were then derived following the methodology described above.

2.4 HPLC pigment data

For pigment analysis, seawater volumes ranging from 700 mL to 1 L were filtered onto 25-mm diameter Whatman GF/F filters and immediately stored at -80 °C until further analysis. Pigments were extracted using 90 % acetone and analysed by High-Performance Liquid Chromatography (HPLC) following the method of Van Heukelem and Thomas (2001). Calibration was performed using pigment standards from DHI Water and Environment (Hørsholm, Denmark). The following pigments were identified (with abbreviations in parentheses): chlorophyll

https://doi.org/10.5194/egusphere-2026-5308
Preprint. Discussion started: 11 September 2026

a (Chl a), fucoxanthin (Fuco), chlorophyll *c1 + c2* (Chl c1.c2), alloxanthin (Allo), antheraxanthin (Anth), beta-carotene (β-Car), chlorophyll *b* (Chl b), chlorophyll *c3* (Chl c3), diadinoxanthin (Diadino), neoxanthin (Neo), peridinin (Perid), and prasinoxanthin (Pras).

2.5 Metabarcoding analysis

For DNA analysis of the pico, nano and micro (< 100 µm) size fractions, 500 mL of seawater was prefiltered through a 100 µm mesh to remove large metazoans, then filtered onto an MF-Millipore MCE membrane filter with a 0.22 µm pore size. Samples were immediately stored at -80 °C until further processing. Microbial DNA was extracted from a total of 140 samples (including four negative extraction controls) using the DNeasy PowerLyzer Microbial Kit (Qiagen, Hilden, Germany) following the manufacturer's protocol. The V4 region of the 18S rRNA gene was amplified using the primer set TAReuk454FWD1 (5'-CCAGCASCYGCGGTAATTCC-3') and the TAReukREV3 (5'-ACTTTCGTTCTTGATYRA-3') (Stoeck et al., 2010). PCRs and library preparation were done as previously described in Meire et al. (Meire et al., 2023). For quality control, blanks and technical replicates were included. Paired-end (2 x 300 base pairs) sequencing was performed with the Illumina MiSeq technology (Illumina, San Diego, US) by Genewiz (Leipzig, Germany). 13,647,731 of raw reads were generated from 150 samples. The high throughput sequence data have been deposited in the NCBI Sequence Read Archive (SRA) under BioProject accession PRJNA1457328.

The 18S Illumina MiSeq data were processed using the DADA2 v. 1.14.1 pipeline (Callahan et al., 2016) in R (R Core Team, 2021). Primers were removed using the 'cutadapt' function. Quality control, trimming, and filtering were performed with the 'filterAndTrim' function, discarding reads with more than two expected errors. Forward and reverse reads were truncated at 250 and 200 nucleotides, respectively. Sequences were dereplicated using the 'derepFastq' function, and Amplicon Sequence Variants (ASVs) were inferred with the 'learnErrors' function. Paired-end reads were merged with a minimum overlap of 20 bp using 'mergePairs', and chimeric sequences were removed with 'removeBimeraDenovo'.

Taxonomic assignment of ASVs was performed using the Protist Ribosomal Reference (PR^2) database v. 5.0.0 (Vaulot et al., 2023) via the 'assignTaxonomy' function, with a minimum bootstrap confidence of 98%. Further ASV processing was conducted using the phyloseq package v. 1.50.0 (McMurdie and Holmes, 2013). Singletons and doubletons were removed to retain genotypes more likely to be ecologically relevant. Contaminants (ASVs with >1% relative abundance in negative controls) were excluded before downstream analysis.

To focus specifically on the phytoplankton community and ensure consistency with pigment-based analyses, a phyloseq object was constructed including only ASVs belonging to taxonomic classes known to contain primarily photosynthetic taxa. The following classes were retained: *Bacillariophyceae*, *Bolidophyceae*, *Chlorophyceae*, *Chrysophyceae*, *Coscinodiscophyceae*, *Cryptophyceae*, *Dictyochophyceae*, *Mamiellophyceae*, *Mediophyceae*, *Nephroselmidophyceae*, *Prasino-Clade-VIII*, *Prasinodermophyceae*, *Prymnesiophyceae*, *Pyramimonadophyceae* and *Trebouxiophyceae*.

2.6 Data analysis

All data and statistical analyses, and data visualizations, were performed in R v. 4.4.2 (R Core Team, 2021). Data visualization and plotting were conducted using the ggplot2 package v. 3.5.1 (Wickham, 2016).

Relationships between the size-based functional groups (carbon biomass) and environmental variables were assessed using Spearman rank correlation analyses due to non-normal data distribution (Shapiro–Wilk test).

https://doi.org/10.5194/egusphere-2026-5308
Preprint. Discussion started: 11 September 2026

Environmental variables were standardized (*z*-scores) prior to analysis, and pairwise correlations were considered significant at $p < 0.05$.

A hierarchical cluster analysis was conducted on the pigment dataset using the dendextend package (Jefferis, 2013). Samples from 150 and 300 m depth were excluded as frequently no pigments could be detected. Prior to analysis, pigment concentrations were normalized to total chlorophyll *a* (TChla), which in this study corresponds to Chl a, as no other Chl a derivatives were detected. Ward's linkage method (based on the inner squared distance) was used, with correlation distance (1 - *r*, where *r* is Pearson's correlation coefficient between phytoplankton normalized pigment data) (Catlett and Siegel, 2018; Latasa and Bidigare, 1998). The resulting dendrogram, based on all normalized pigment data, was divided into distinct taxonomic clusters using a linkage cutoff distance of 0.7. To evaluate the validity of the hierarchical cluster analysis, the cophenetic correlation coefficient and *p*-values were computed (Legendre and Legendre, 2012). The cophenetic correlation coefficient compares the original distance matrix from the cluster analysis with the linkage distances used to construct the dendrogram. Values range from 0 to 1, with values closer to 1 indicating a high correlation between the distances, suggesting that the dendrogram accurately represents the relationships between input parameters (the normalized pigment data). A *p*-value of <0.05 was considered statistically significant.

An Empirical Orthogonal Function (EOF) analysis was performed on the pigment dataset via wql package (Jassby, 2017) to evaluate covariation between pigment groups (Catlett and Siegel, 2018; Kramer and Siegel, 2019). This analysis decomposes the dataset into dominant orthogonal functions that describe the major modes of variability in the pigment data. The percentage of variance explained by each mode decreases with higher modes; thus, Mode 1 accounts for the greatest variance, and only the first few modes are useful for data interpretation. For each mode, the EOF analysis produces both loadings for the input variables (i.e. correlations between an EOF mode and the normalized pigment data) and amplitude functions (AFs, i.e. how much each mode contributes to the observed variability in a sample) for each sample. The original dataset can be reconstructed by summing the product of the loadings and AFs over all EOF modes. Before conducting the EOF analysis, pigment concentrations (normalized to TChla) were *z*-score transformed. Correlations between the dominant EOF modes and various environmental parameters—including Chl a, temperature, salinity, PAR, turbidity and inorganic nutrient concentrations—were assessed.

For diversity analysis of the metabarcoding data, read depths were rarefied to the lowest sample count using phyloseq (McMurdie and Holmes, 2013), retaining singletons. Alpha diversity was assessed using the Shannon index (H') via the 'diversity' function in the vegan package (Oksanen et al., 2025). Seasonal and fjord-specific differences were tested with the Wilcoxon rank-sum test, whereas spatial variation among stations was assessed by averaging Shannon diversity across depths per station and applying the Kruskal–Wallis test. A constrained analysis of principal coordinates (CAP) was conducted to evaluate how environmental variables are related to phytoplankton community composition (metabarcoding data), using the 'capscale' function (Anderson and Willis, 2003) in the vegan package (Oksanen et al., 2025). The data were Hellinger-transformed, and environmental variables were standardized using *z*-scores. To reduce multicollinearity of environmental variables, variance inflation factors (VIFs) were assessed using the 'vif.cca' function, and variables with VIF > 10 were excluded (Borcard et al., 2018). Constraining variables were then selected through forward selection using the 'ordiR2step' function from the vegan package (Oksanen et al., 2025). The significance of the CAP model and individual explanatory variables was tested via permutation tests (999 permutations). The top 15 ASVs contributing most to

https://doi.org/10.5194/egusphere-2026-5308
Preprint. Discussion started: 11 September 2026

the multivariate structure—identified based on the highest loadings on the first two CAP axes—were visualized in the ordination plots. Taxa were presented at the genus level, with the corresponding ASV identifier indicated.

3 Results

3.1 Physico–chemical environment, nutrients, fluorescence (Chl a), and primary production

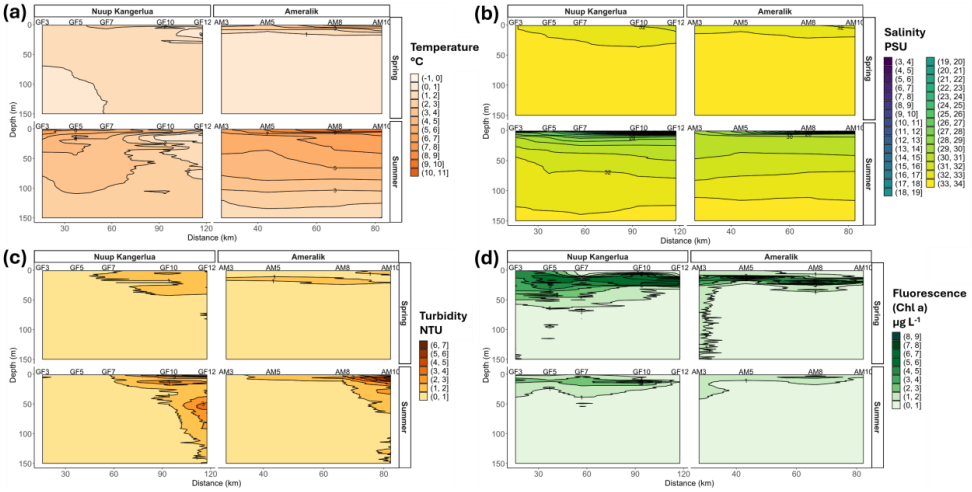

Figure 2: *(a) Temperature (°C), (b) salinity (PSU), (c) turbidity (NTU) and (d) fluorescence calibrated to Chl a (µg L^{-1}) in the upper 150 m; from outer to inner fjord transects in NK and AM in spring (top) and summer (bottom). Distance to fjord mouth indicated on x-axis; Location of stations indicated on second x-axis.*

Average spring water temperature was 1.3 °C in NK and 1.6 °C in AM, with surface maxima of 3 °C and 6 °C respectively in inner NK and AM (Fig. 2a). A weak thermocline developed between 1–10 m depth in the mid-inner reaches of both fjords. Surface water salinity decreased from ~33 in the outer to ~31 in the inner fjords (Fig. 2b), with limited stratification. Turbidity was low in both fjords (average NTU ~ 0.7 in AM and ~ 0.8 in NK). In summer, the two fjords exhibited contrasting temperature distributions. In NK, maximum surface temperatures reached 8 °C at the outer station (GF3) and gradually decreased towards the inner fjord. The coldest waters occurred between 10 and 20 m depth, reaching 0 °C, while surface temperatures at GF10 and GF12 remained around 3 °C and sub-surface waters were ≤ 2 °C throughout most of the water column (Fig. 2a). In contrast, AM was characterized by generally warmer conditions, with surface temperatures reaching up to 10 °C at stations AM8–AM10. Both fjords also exhibited pronounced vertical gradients in salinity and density anomaly during summer (Figs. 2b, S4a). In NK, the lowest salinity and density anomaly values were observed at the innermost stations, indicating strong but spatially localized surface freshening. In AM, low-density surface waters were distributed across a larger fraction of the transect and were associated with relatively uniform upper-water-column conditions. Consequently, stratified conditions were present in both systems, but differed in their spatial expression, being concentrated in the inner fjord in NK and extending over a broader portion of the transect in AM. In both fjords, salinity was lowest in surface waters and increased rapidly with depth. Surface salinity reached minima of approximately 3 in the inner NK stations and 12 in the inner AM stations, while deeper waters were characterized by substantially higher salinities throughout the fjords. An up-fjord turbidity gradient was present

https://doi.org/10.5194/egusphere-2026-5308
Preprint. Discussion started: 11 September 2026

in both systems (Fig. 2c; Fig. S4b), with turbidity reaching its maximum (~6 NTU) at 10 m in AM (AM10) and below the surface (~5 NTU) in inner NK, with a local maximum at depth. Chl a concentrations were higher in spring than in summer, with overall lower values in AM than in NK (Fig. 2d, Fig. 3). During spring, distinct subsurface peaks were observed at 10–20 m depth in NK (~7 µg L^{-1}, GF10 and GF12) and AM (~5 µg L^{-1}, AM8), while in outer NK (GF3–GF5), concentrations were also higher in the surface layers. In AM, concentrations decreased up-fjord (AM3 ~2 µg L^{-1}, AM10 ~1 µg L^{-1}). In summer, the DCM was deeper and more distinct in NK (~10–20 m; fjord average ~2.8 µg L^{-1}) than AM (~1–10 m; ~1.9 µg L^{-1}). Peak summer values reached 4.5 µg L^{-1} at 14 m in GF10 and ~3 µg L^{-1} at 5 m in AM8.

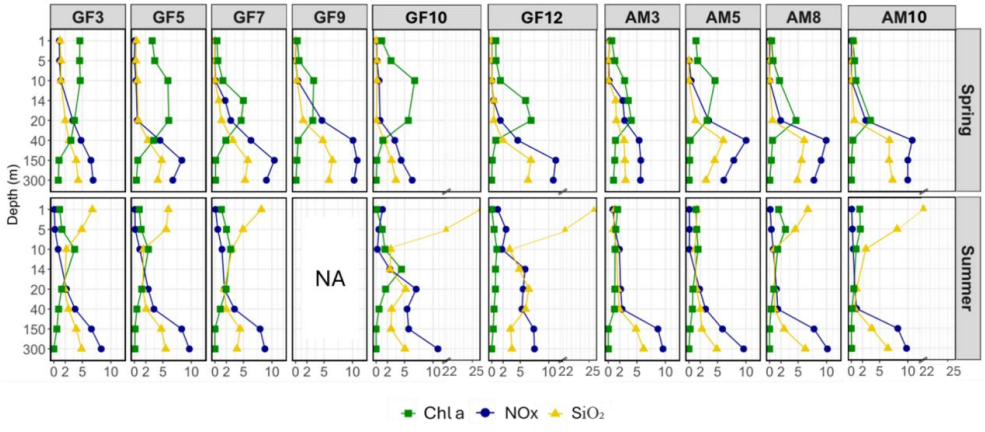

Figure 3: *Depth profiles of Chl a (µg L^{-1}, green line), nitrate + nitrite (NOx, µM, blue line), and silicate (SiO_2, µM, yellow line) in the upper 300 m of NK (GFx) and AM (AMx) in spring (top) and summer (bottom). Note x-axis truncated (10-22) in GF10, GF12 and AM10. Note that the y-axis is not to scale.*

In spring, NOx and silicate were fully depleted in the upper 10 m of both fjords, with the exception of GF3, where concentrations reached ~ 1 µM for both nutrients (Fig. 3; Fig. S5a–b). Between 10-20 m, NOx concentrations increased (max 4.5 µM in GF9), but silicate remained < 2 µM, especially in the inner fjords, resulting in average Si:N ratios of approximately 8:16. Below 40 m, nutrient concentrations increased, reaching their highest levels in inner NK (GF12, NOx > 10 µM, SiO_2 > 6 µM). In summer, silicate was abundant in surface waters (1–5 m) in both fjords, except in outer AM (Fig. 3; Fig. S5b). The highest concentrations were recorded in the inner fjords (~21 µM at GF12, ~13 µM at AM10). In contrast, NOx remained very low (<0.3 µM) in the surface layer, except at GF10 and GF12 (~2 µM, Fig. 3; Fig. S3a). NOx increased between 14–40 m in NK (~4 µM), whereas in AM it remained < 2 µM throughout the upper water column. Below 150 m, both fjords exhibited NOx concentrations ~ 8 µM, with silicate levels approximately half those. Phosphate followed a similar vertical pattern to NOx, with a mean concentration of ~0.3 µM across depths and seasons (Fig. S3c). Ammonium levels were consistently higher in summer than spring, except at GF3 (Fig. S3d), with levels gradually increasing up-fjord, peaking between 10-40 m in the innermost stations (on average ~2.1 in AM and ~1.3 in NK).

In spring, silicate was the limiting nutrient in both fjords (Si/N = 15:16; Fig. S6a; S7) (Brzezinski, 1985). In summer, nitrogen became limiting in the surface waters, but below ~ 14 m in NK and ~40 m in AM, NOx

https://doi.org/10.5194/egusphere-2026-5308
Preprint. Discussion started: 11 September 2026

concentrations increased and silicate again became the limiting nutrient (Fig. S6a; S7). Phosphate was not limiting relative to nitrogen, as the N:P ratio consistently remained below 16:1 (Fig. S6b) (Redfield, 1934, 1958).

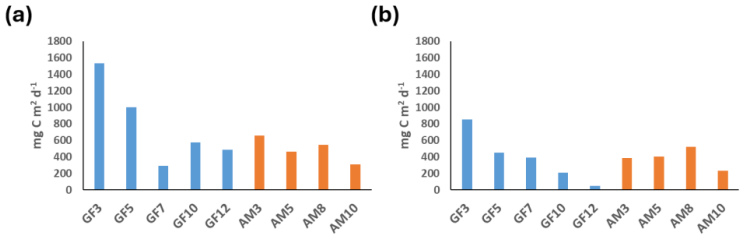

Figure 4. *Depth-integrated primary production (0–50 m; mg C m⁻² d⁻¹) in Nuup Kangerlua (GFx, blue) and Ameralik (AMx, red) during (a) spring and (b) summer; outer (GF3, AM3) to inner fjord (GF12, AM10).*

Depth-integrated primary production (PP) rates in spring were overall higher in NK than AM, with highest values in the outer fjord (GF3, ~1500 mg C m⁻² d⁻¹) and an up-fjord decrease (GF7–GF12, ~300–600 mg C m⁻² d⁻¹, Fig. 4a). In contrast, AM displayed overall lower and more homogeneous PP values (~300 to 650 mg C m⁻² d⁻¹). In summer (Fig. 4b), PP decreased substantially in NK across most stations, with values generally < ~500 mg C m⁻² d⁻¹ and particularly low rates at GF12. In AM, PP was comparable to or slightly lower than in spring, with a peak at AM8 (~500 mg C m⁻² d⁻¹).

https://doi.org/10.5194/egusphere-2026-5308
Preprint. Discussion started: 11 September 2026

3.2 Spatial and seasonal distribution of phytoplankton size classes: abundance, biomass and relation with environmental factors

(i) Phytoplankton < 100 µm (iFCM)

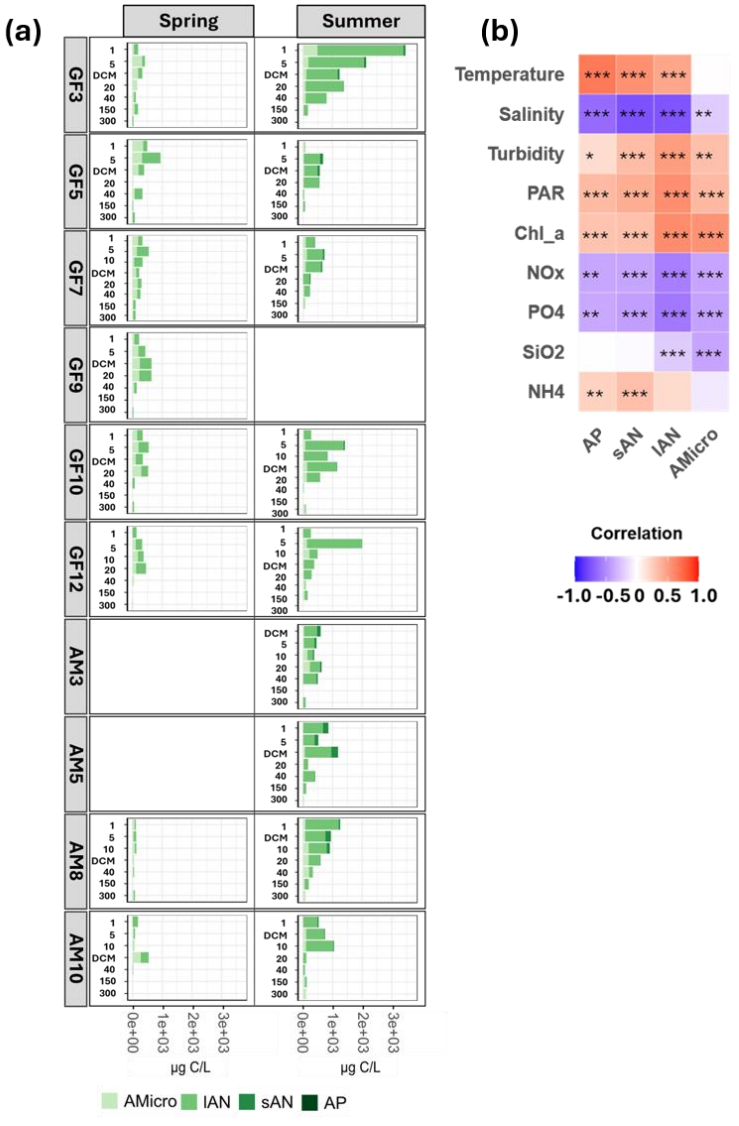

Figure 5: *(a) Carbon biomass (µg C L⁻¹) of phytoplankton size classes in the < 100 µm fraction versus depth in NK (GFx) and AM (AMx) in spring (left) and summer (right). DCM = deep chlorophyll maximum. AP – picophytoplankton, sAN – small nanophytoplankton, lAN – large nanophytoplankton and AMicro – microphytoplankton. The AP fraction is hardly discernible in the plot due to its very low carbon biomass relative to the plotting scale. (b) Spearman's correlation heatmap of size class carbon biomass and environmental variables. ***p ≤ 0.001;**p ≤ 0.005;*p ≤ 0.05.*

https://doi.org/10.5194/egusphere-2026-5308
Preprint. Discussion started: 11 September 2026

Trends in cell numbers are described in Supplementary sect. S3.

In spring, carbon biomass of phytoplankton < 100 µm was always codominated by lAN and AMicro (Fig. 5a). Average biomass across depths and stations was lower in inner AM (AM8–AM10; ~100 µg C L^{-1}) compared to NK (~260 µg C L^{-1}).

In summer, biomass became strongly dominated by lAN, which was > 3x higher in summer (overall average ~580 µg C L^{-1}) than in spring (~160 µg C L^{-1}) in the upper 40 m (Fig. 5a). Biomass was generally similar between fjords, except for pronounced peaks in GF3 (1–5 m; ~2.8 × 10^3 µg C L^{-1}) and in GF12 (5 m, ~2 × 10^3 µg C L^{-1}). sAN also exhibited higher biomass in summer than in spring, particularly in AM, where it averaged ~70 µg C L^{-1} in the upper 40 m (~27 µg C L^{-1} in NK). AP biomass was very low, averaging ~1.2 µg C L^{-1} in AM and ~0.2 µg C L^{-1} in NK. In contrast, AMicro biomass was slightly higher in NK than in AM, with mean values of ~79 and ~68 µg C L^{-1}, respectively (Fig. 5a). Total biomass of AP, sAN, and lAN was strongly positively correlated with temperature and negatively with salinity (Fig. 5b); AP and sAN also showed a moderate positive correlation with NH_4^+. lAN and AMicro biomass was strongly positively correlated with Chl a and negatively with SiO_2. lAN also exhibited strong positive correlations with turbidity and PAR (both higher in summer), and strong negative correlations with NOx and PO_4^{3-} compared to the other functional groups.

(ii) Microplankton (100-300 µm, FlowCAM)

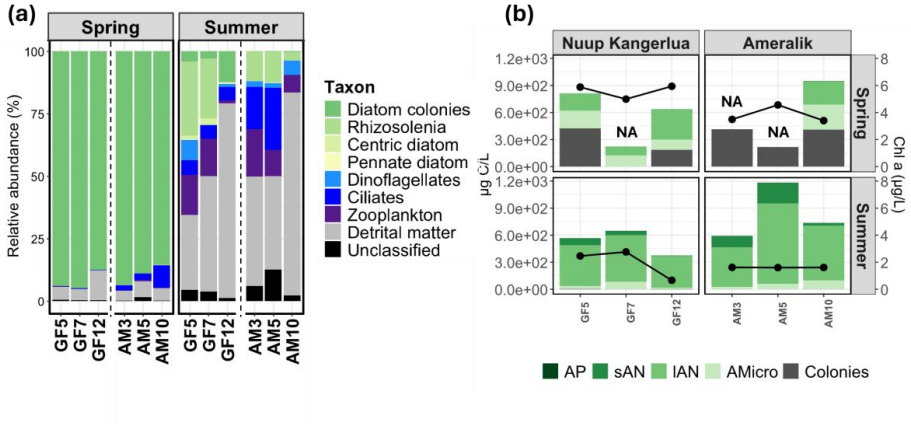

Figure 6: *(a) Bar plots showing the relative particle abundances (%) of 100–300 µm planktonic and other suspended particles detected by FlowCAM analysis from the deep chlorophyll maximum (DCM) during spring and summer in NK (GFx) and AM (AMx). (b) Total carbon biomass (µg C/L) of phytoplankton classes < 100 µm (iFCM, green) and diatom colonies (100-300 µm, FlowCAM, grey) at the DCM in spring (top) and summer (bottom). Black circles and lines indicate chlorophyll a concentrations (µg L^{-1}) at the DCM, shown on the secondary y-axis. Data not available (NA) for GF7 spring (FlowCAM), AM3 and AM5 spring (iFCM).*

In spring, the 100–300 µm plankton fraction at the DCM in both fjords was largely dominated by diatom colonies, accounting for ~90 % of the cell counts (Fig. 6a). Cell concentrations reached ~ 1 × 10^3 cells mL^{-1} in GF5, AM3, and AM10, corresponding to biomasses of 424, 414, and 410 µg C L^{-1}, respectively (Fig. 6b; S9). Lower values were observed in GF12 and AM5 (~5 × 10^2 and ~7,5 × 10^2 cells mL^{-1}, and 185 and 217 µg C L^{-1} respectively,

https://doi.org/10.5194/egusphere-2026-5308
Preprint. Discussion started: 11 September 2026

Fig. 6b; S9). Ciliates represented the second most abundant group in AM, contributing ~2 % at AM3–AM5 and ~9 % at AM10, whereas they accounted for < 1 % in NK. In summer, diatom colonies represented only 6, 3 and 12 % respectively in GF5, GF7 and GF12, and less than 0.5 % in AM. Their biomass declined sharply, with the highest values recorded in NK, particularly in GF5 (4.4 µg C L^{-1}), with values in AM close to zero (Fig. 6b). Note that the contribution of colonies and microplankton to total phytoplankton biomass in summer was much lower (hardly detectable in Fig. 6b) than that of the nanophytoplankton. Among diatoms, *Rhizosolenia* sp. showed a higher relative abundance during summer, particularly in GF5 and GF7 (~25 %). Unfortunately, its contribution to total biomass could not be quantified as cells were fragmented. Dinoflagellates peaked at GF5 (~8 %) and AM10 (~6 %), while ciliates became important in AM3 and AM5 (~20 %). Zooplankton contributed ~15 % in GF5–GF7 and ~1 % in GF12, decreasing from ~19 % at AM3 to ~7 % at AM10. In the innermost stations of both fjords, detrital material represented the dominant component (>75 %) in the 100–300 µm fraction.

3.3 Phytoplankton pigments

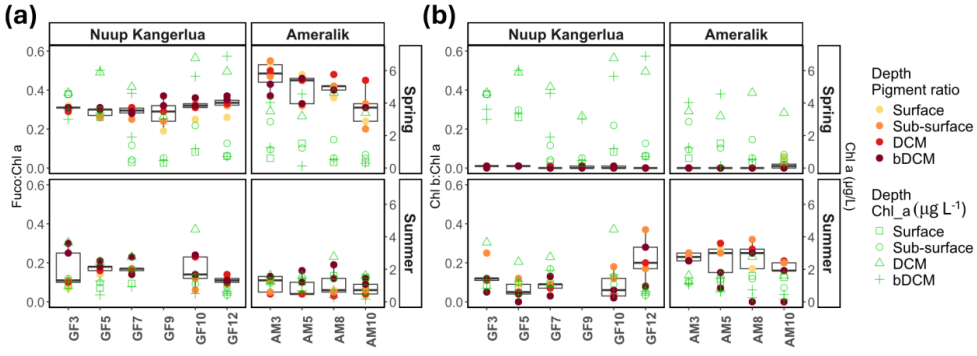

Figure 7: *(a) Fuco to Chl a ratio; (b) Chl b to Chl a ratio in NK (left a-b) and AM (right a-b) in spring (top) and summer (bottom). Colors represent sampling depths. Green shapes show Chl a concentration (µg L^{-1}) at sampling depths. Sampling depths: surface (1 m; yellow; rectangle), sub-surface (5, 10 m; light-orange; circle), deep chlorophyll maximum (DCM; red; triangle), below DCM (bDCM, 20, 40 m; brown; plus).*

Fucoxanthin (Fuco) was the dominant accessory pigment during spring, especially in surface waters of GF10 and GF12 (~2 µg L^{-1}; Fig. S10), mirroring the distribution of Chl a. The Fuco/Chl a ratio, a proxy for the importance of diatoms (Vidussi et al., 2001), was slightly higher in AM than NK, especially in the outer fjord (Fig 7a). Neoxanthin (Neo), prasinoxanthin (Pras) and peridinin (Perid) were not detected during spring (Fig. S10). The Chl b/Chl a ratio, an indicator of the importance of green algae (Jeffrey et al., 2011), was ~ 0 in most stations except for very low values in outer NK (GF3-GF5) and inner AM (AM10; Fig 7b). During summer, Fuco concentrations declined markedly along with Chl a, with the highest Fuco levels found at the DCM in station GF10 (~1 µg L^{-1}; Fig. S10). The Fuco/Chl a ratio, albeit overall much lower than in spring, were higher in NK than AM (Fig. 7a). Antheraxanthin (Anth) was not detected in summer samples. Its exclusive detection in spring is consistent with light-stress responses previously reported in diatoms (Blommaert et al., 2017; Lohr and Wilhelm, 2001). Chl b became the dominant accessory pigment, with Chl b/Chl a ratios being overall higher than in spring, especially in AM (Fig. S10), except at GF12 (10 m; Fig. 7b).

https://doi.org/10.5194/egusphere-2026-5308
Preprint. Discussion started: 11 September 2026

Hierarchical cluster analysis of pigment concentrations normalized to TChl a (see Supplementary section S4 and Fig. S11 for details) revealed three distinct clusters, namely (i) diatoms, (ii) haptophytes, and (iii) green algae, dinoflagellates and cryptophytes. These main groups can also be recognized in the EOF analyses, which was used to identify the major modes of variability in qualitative pigment composition in the study area.

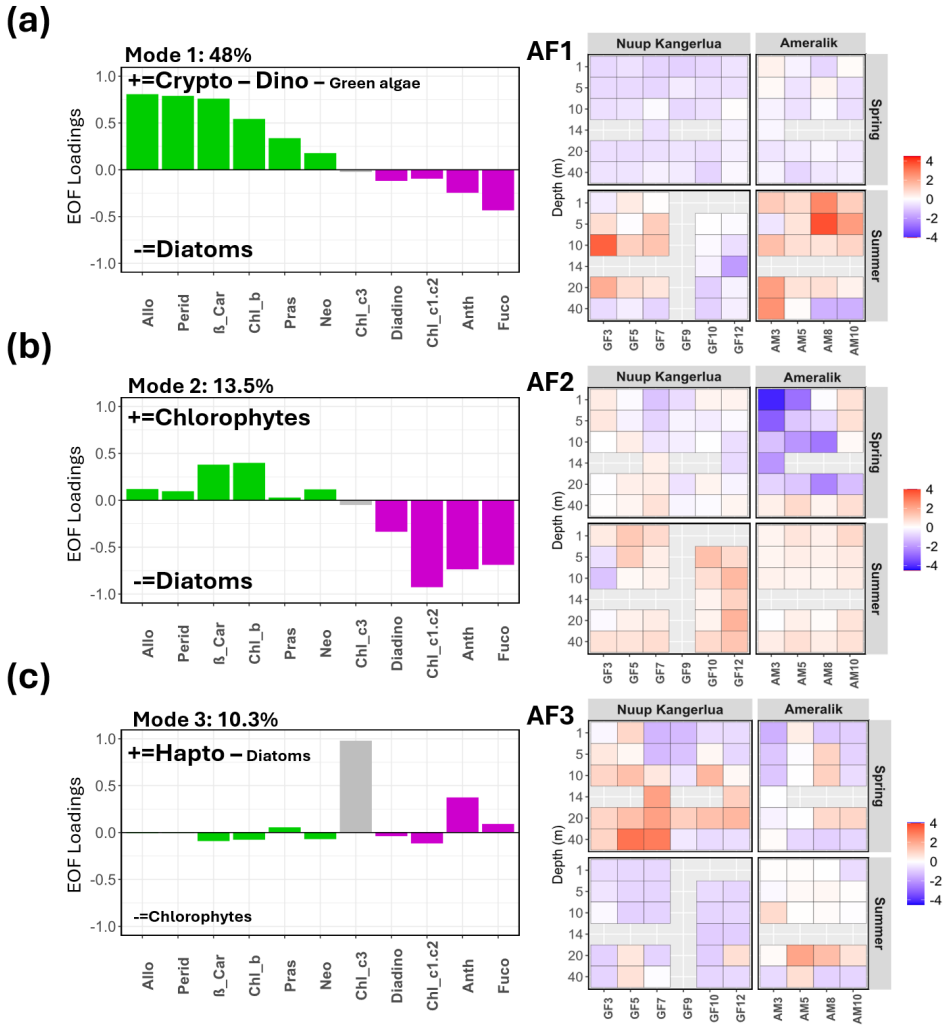

Figure 8: *Empirical orthogonal functions for Mode 1 (a), 2 (b) and 3 (c) calculated for phytoplankton pigment ratios to TChla concentration. Phytoplankton taxa abbreviation: crypto (cryptophytes), dino (dinoflagellates), hapto (haptophytes). Loadings are coloured based on pigment clusters (Fig. 11): green – diverse community; grey – haptophytes; magenta – diatoms. Amplitude function (AF) magnitude is indicated as positive (red) or negative (blue) for each sample. Background grid cells indicate missing values (NA).*

The first three EOF modes together explain 71.8 % of the total variance in the dataset (Fig. 8).

https://doi.org/10.5194/egusphere-2026-5308
Preprint. Discussion started: 11 September 2026

EOF Mode 1, explaining 48 % of the total variance, separates communities dominated by cryptophytes (Allo), dinoflagellates (Perid), chlorophytes (Chl b, β-Car), and prasinophytes (Pras, Neo) from diatom-dominated assemblages (Fig. 8a). This mode is most negative in spring, particularly in NK, and most positive in summer, except in inner NK where instead diatoms remain important. It shows a strong positive correlation with temperature and a negative one with salinity (Tab. S3). EOF Mode 2 explains 13.5 % of the variance and separates chlorophytes (positive) from diatoms (negative, Fig. 8b). It is overall more negative in spring (especially in outer AM), and more positive in summer, notably at station GF12 below 10 m. This mode is positively correlated with inorganic nutrients, especially silicate (Tab. S3). EOF Mode 3, accounting for 10.3 % of the total variability, is strongly positively correlated with haptophytes and to a lesser extent with diatoms, while being weakly negatively correlated with chlorophytes (Fig. 8c). This mode is most positive in spring at 10–40 m depth in NK (stations GF5 and GF7), and becomes more negative in surface (1-5 m) spring waters and in summer throughout NK. Mode 3 is correlated positively with Chl a (Tab. S3).

https://doi.org/10.5194/egusphere-2026-5308
Preprint. Discussion started: 11 September 2026

3.4 DNA metabarcoding

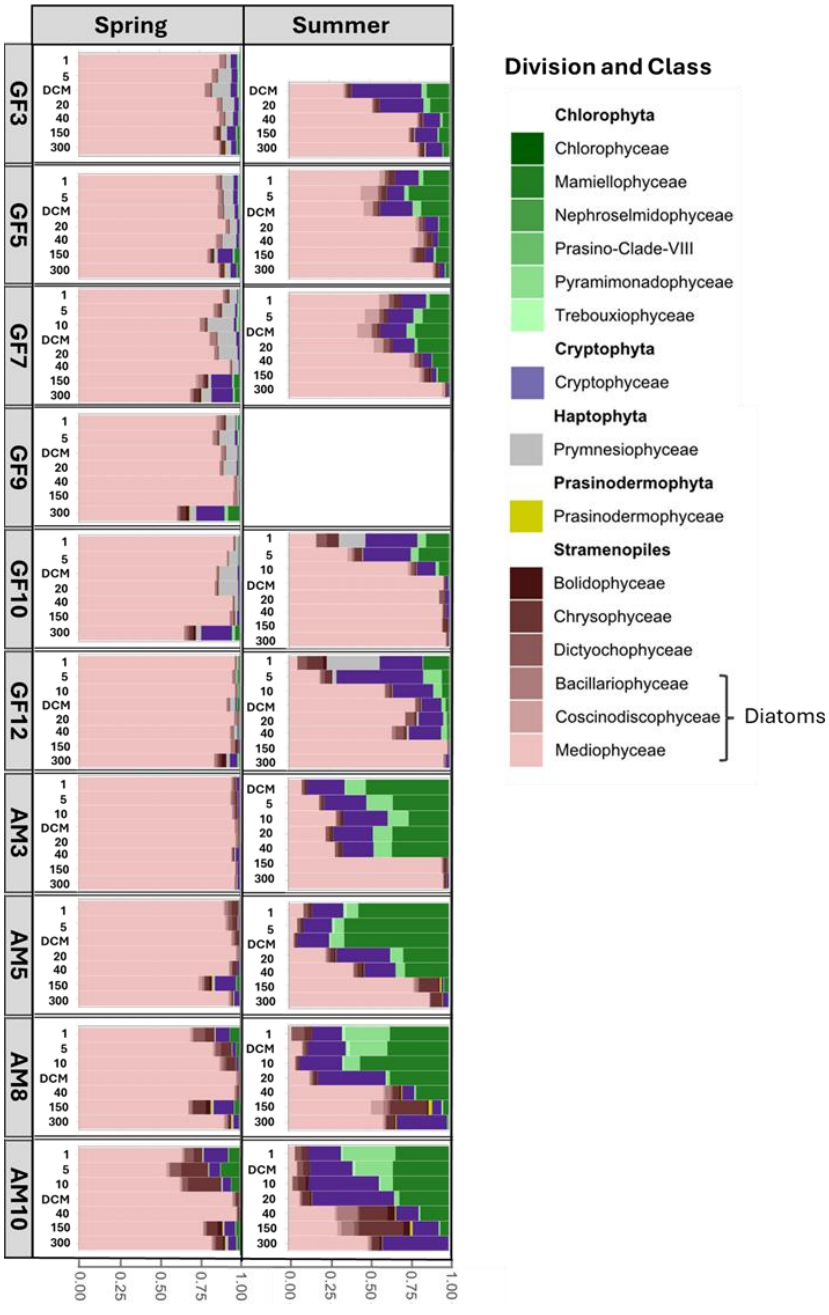

Figure 9: *Phytoplankton relative abundances based on metabarcoding data at discrete sampling depths and stations in NK (GFx) and AM (AM) in spring (left) and summer (right) from outer (GF3, AM3) to the inner fjord (GF12, AM10). DCM indicates deep chlorophyll maximum.*

https://doi.org/10.5194/egusphere-2026-5308
Preprint. Discussion started: 11 September 2026

The 18S rRNA metabarcoding dataset yielded 1,523 ASVs, derived from 3,349,541 reads across 136 samples, which could be assigned to phytoplankton groups. Dinophyceae ASVs were excluded from our phytoplankton-focused analyses (except for pigment-related signals, cf. above) for reasons outlined in Supplementary Sect. S1 and Figs. S1–S2, resulting in a final phytoplankton dataset of 648 ASVs (1,287,140 reads). Shannon diversity of the rarefied dataset (Fig. S3) showed no significant spatial (average H′ per station across depths) or seasonal differences. However, during summer, AM exhibited significantly higher Shannon diversity than NK (Wilcoxon test, $p < 0.05$).

In spring, communities in both fjords were dominated by diatoms (class Mediophyceae, on average 86 % of total relative read abundance across all samples, Fig. 9). *Chaetoceros* was the most prevalent genus, with an average abundance of 57 % in AM and 42 % in NK, followed by *Thalassiosira* (38 % in NK and 21 % in AM) and *Porosira* (8 % in AM and 2 % in NK). In NK, diatom relative abundance (upper 40 m) increased up-fjord, while in AM the opposite was observed. Haptophyta (mainly *Phaeocystis* cf. *pouchetii*) represented the second most abundant group in NK (5 % of reads), but not in AM (0.2 %). Cryptophyta, mainly *Teleaulax*, contributed on average 2 % in NK and 3 % in AM, peaking at ~4 % at station AM10 in the upper 40 m. Its relative abundance increased with depth, reaching ~5 % on average between 150 and 300 m in both fjords. Inner AM (AM8–10) communities were distinct, holding several phytoplankton groups that were virtually absent elsewhere. Chrysophyceae, mainly the mixotroph *Dinobryon*, reached ~9 % relative abundance in inner AM. Similarly, Dictyochophyceae (mainly *Pseudopedinella*) as well increased towards inner AM (~3 %). Among Chlorophyta, *Micromonas* (class Mamiellophyceae) emerged as the dominant genus (~5 % in AM10).

In summer, the relative importance of diatoms (Mediophyceae) was markedly lower in AM (on average 30 %) but remained high in NK (on average 66 %). *Chaetoceros* again was the most abundant genus, comprising 48 % in NK and 17 % in AM. *Skeletonema* accounted for 8 % in both fjords, while *Thalassiosira* made up 8 % in NK but only 1 % in AM. *Rhizosolenia* (Coscinodiscophyceae) accounted for ~6 % of the relative abundance in the upper 40 m at mid-fjord stations in NK (GF5–GF7), while remaining < 1 % elsewhere. The green algal Mamiellophyceae, mainly represented by *Ostreococcus*, *Micromonas* and *Bathycoccus,* became highly prominent in summer, particularly in AM, where they accounted for 28 % of the community compared to 9 % in NK. Pyramimonadophyceae also were an important component of the community (on average 8 % in AM vs 2 % in NK), with *Pyramimonas* as the dominant genus, and unidentified *Pyramimonadales* reaching 25 % in surface waters at AM10. Cryptophyceae followed a similar pattern (21 % in AM and 13 % in NK), dominated by *Plagioselmis*, *Teleaulax*, *Baffinella* and *Rhodomonas*. Notably, *Hemiselmis* reached ~5 % of the community in AM10 surface waters but remained <1 % elsewhere. The haptophyte *Pseudohaptolina* was exclusively detected at GF10 and GF12, peaking at 1 m depth with 16 % and 32 % of total reads, respectively. The dictyochophyte *Florenciella*, absent in AM, increased toward inner NK, reaching 3 % in the upper 40 m at GF12, while *Pseudopedinella* represented ~2 % of the community in both fjords. Finally, Chrysophyceae were relatively abundant in deeper waters (40–300 m) of inner AM (AM8–AM10), mainly belonging to mixotrophic (*Dinobryon*, ~3 %) or heterotrophic (*Paraphysomonas*, ~9 %) genera.

https://doi.org/10.5194/egusphere-2026-5308
Preprint. Discussion started: 11 September 2026

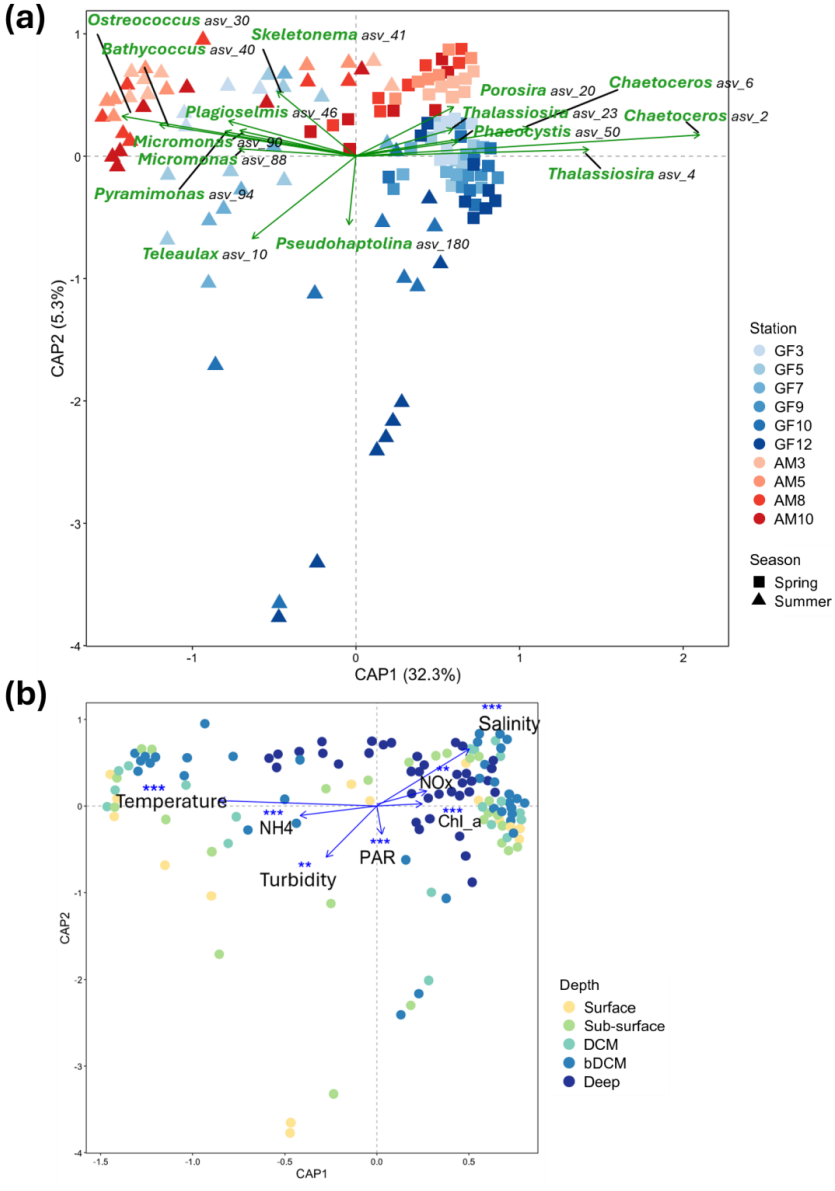

Figure 10: *(a-b) Constrained analysis of principal coordinates (CAP) ordination diagram showing phytoplankton community variation based on metabarcoding data (ASVs level). (a) Sample symbol colour refers to station and shape to season; the most important taxa are shown as green vectors. (b) Biplot of sample depths: surface (1 m yellow), sub-surface (5, 10 m light-green), deep chlorophyll maximum (DCM, cyan), below DCM (bDCM, 20, 40 m, blue), and deep (150, 300 m, dark blue); blue arrows represent the selected environmental variables; stars indicate the significance of permutation tests: *** $p \leq 0.001$, ** $p \leq 0.005$.*

https://doi.org/10.5194/egusphere-2026-5308
Preprint. Discussion started: 11 September 2026

The constrained analysis of principal coordinates (CAP) explained 46 % of the variance in phytoplankton community composition (adjusted R^2 = 0.43, $p < 0.001$). Environmental variables selected through forward selection included temperature, salinity, turbidity, NOx, NH_4^+, Chl a, and PAR. CAP1, which explained 32.3 % of the total variance, was positively correlated with salinity and strongly negatively correlated with temperature and, to a lesser extent, NH_4^+ (Fig. 10b). *Chaetoceros*, *Thalassiosira*, *Porosira*, and *Phaeocystis* were associated with the positive side of CAP1, whereas *Ostreococcus*, *Bathycoccus*, *Pyramimonas*, *Plagioselmis*, *Skeletonema* and *Micromonas* aligned with the negative side. This axis primarily distinguished spring from summer communities. Within the spring cluster, AM and NK samples were segregated, with AM characterized by slightly higher salinity and lower turbidity, and NK samples by higher Chl a. Surface spring samples from inner AM where slightly more similar to the summer samples. While no pronounced depth differentiation in community structure was observed in spring, in summer deep samples (below DCM, but especially 150 and 300 m) became clearly differentiated from the other samples, showing more affiliation with the spring communities because of the prominent diatom signal. Along the second axis (CAP2, 5.3 % of the variance), the summer surface to bDCM samples from the inner GF stations, being characterized by higher importance of *Teleaulax* and especially *Pseudohaptolina*, were separated from the other summer samples (Fig. 10b).

4 Discussion

While the divergent impact of glacier type (MTG vs LTG) on phytoplankton community structure, biomass and primary production (PP) is increasingly recognized (Chitkara et al., 2024; Dąbrowska et al., 2025; Kanna et al., 2022; Meire et al., 2023; Stuart-Lee et al., 2023), little information is as yet available on the size structure and taxonomic composition of the smaller components of the phytoplankton, with previous studies mainly focusing on the microplankton (Chitkara et al., 2024; Dąbrowska et al., 2025; Kanna et al., 2022). In this study, we used a combination of complementary high-throughput imaging (imaging flow cytometry, FlowCAM), HPLC pigment and high taxonomic resolution (18S rRNA metabarcoding) tools to detail seasonal contrasts in phytoplankton community structure in two Arctic fjord systems influenced by different glacier types, with specific focus on the smaller size components (pico-, nano- and microphytoplankton < 300 µm). Our results support the above-mentioned general seasonal divergence in community structure related to contrasting glacial influences and water-column structures, with diatoms persisting in parts of the MTG-impacted fjord, and small-celled species becoming dominant in the LTG-fjord. Our analyses however additionally revealed that: (1) summer phytoplankton biomass in the LTG but also the MTG fjord became markedly dominated by nanophytoplankton; (2) while in summer diatoms persisted in the MTG fjord (most likely related to enhanced subsurface vertical mixing via subglacial discharge), green algae but also cryptophytes became dominant in the LTG fjord; (3) mixotrophic strategies were promoted in the highly stratified and nutrient- and light-limited surface waters of the LTG fjord; and (4) the surface layers in the innermost stations of the MTG fjord supported a highly distinct community likely shaped by ice mélange conditions, dominated by a potentially harmful, sea ice associated haptophyte species. Below, these findings are described in more detail.

4.1 Chain-forming diatoms dominate spring blooms irrespective of fjord type

In spring, both fjords were characterized by cold surface waters with low turbidity and weak salinity and temperature stratification, indicative of limited freshwater input during the pre-melt season in high-latitude fjords (Meire et al., 2016b; Mortensen et al., 2011, 2013, 2014; Stuart-Lee et al., 2021). Surface waters were strongly depleted in NOx and silicate, and were Si-limited (Si/N ~ 8:16 below 10 m; Fig. S6a), suggesting that the spring

https://doi.org/10.5194/egusphere-2026-5308
Preprint. Discussion started: 11 September 2026

bloom, mainly consisting of diatoms (see below), had depleted nutrients and was close to its decline phase. Indeed, Chl a and primary production (PP) values in the inner part of both fjords were overall lower than those reported for spring blooms in earlier years (Meire et al., 2023; Stuart-Lee et al., 2023). In the outer part of NK, PP values were higher and similar to those reported by Juul-Pedersen et al. (2015) for the 2006–2012 monitoring period. These authors argued this may partly reflect advection of phytoplankton from more stable inner fjord waters to strongly tidally mixed waters in the outer basin (Mortensen et al., 2011), which is consistent with the more vertically homogeneous distribution of Chl a at this site, despite the values being lower than in the rest of the fjord.

In both fjords, the blooms were dominated by microphytoplankton, in particular chain-forming diatoms such as *Chaetoceros* and *Thalassiosira*, which are typical of Arctic spring blooms (Chitkara et al., 2024; Dąbrowska et al., 2025; Hegseth et al., 2019; Krawczyk et al., 2018). The colonial haptophyte *Phaeocystis cf. pouchetii* was also important in the outer and mid-fjord assemblages in NK, consistent with previous studies in Arctic fjords (Chitkara et al., 2024; Krawczyk et al., 2015, 2018). Although *Phaeocystis* blooms in temperate coastal systems are often reported after diatom blooms under low-silicate conditions (Egge and Aksnes, 1992; Peperzak et al., 1998; Smith and Trimborn, 2024), recent observations from Arctic fjords indicate that low silicate is not necessarily a prerequisite, and that mixed-layer depth, light availability, and the abundance and composition of the initial inoculum (i.e. the phytoplankton community present before bloom initiation) may influence its development (Assmy et al., 2023). In our study, *Phaeocystis* was only important in NK, suggesting that local hydrographic or biological controls limited its development in AM. Spatial trends differed between fjords in spring. In NK, the relative importance of diatoms increased up-fjord, whereas in AM the opposite pattern was observed, with the inner stations uniquely hosting a more heterogeneous assemblage characterised by mixotrophic flagellates, including *Dinobryon* and *Pseudopedinella*, and small green algae (*Micromonas*). The colonial chrysophyte *D. balticum* is a common constituent of microplankton communities in Arctic and sub-Arctic coastal areas (Dvoretsky and Dvoretsky, 2024; Rytter Hasle and Riddervold Heimdal, 1998; Stoecker and Lavrentyev, 2018), including NK, where it can reach relative abundances of up to ~ 25 % (Krawczyk et al., 2015). It is often associated with low-irradiance conditions (McKenrie et al., 1995). Although *D. balticum* possesses plastids, it supplements its nutrition through bacterivory (McKenrie et al., 1995). Likewise, heterotrophic nutrition in the dictyochophyte *Pseudopedinella* has been long recognized (Havskum and Riemann, 1996; Sekiguchi et al., 2003), although its presence in the Arctic has rarely been reported (Assmy et al., 2023; Balzano et al., 2012; Lovejoy et al., 2006). *Micromonas* spp. are widely distributed picoplanktonic prasinophytes that are often dominant in Arctic and sub-Arctic pico-phytoplankton communities, particularly under oligotrophic summer conditions (Freyria et al., 2021; Hegseth et al., 2019; Lovejoy et al., 2007). Mixotrophy in *Micromonas* has been suspected, with transcriptomic evidence suggesting intracellular digestion (McKie-Krisberg et al., 2018; McKie-Krisberg and Sanders, 2014), but recent studies have not confirmed prey ingestion or genomic markers typically associated with phagocytosis (Jimenez et al., 2021). Taken together, the occurrence of taxa capable of flexible trophic strategies in inner AM during spring suggest the onset of more stratified, light- and nutrient-limited conditions, characteristic of summer (see below).

4.2 Glacier type drives summer divergence in phytoplankton community structure

During summer, increased meltwater discharge resulted in pronounced haloclines in the inner regions of both fjords. However, while in AM stratification was further reinforced by a distinct thermocline due to solar warming

https://doi.org/10.5194/egusphere-2026-5308
Preprint. Discussion started: 11 September 2026

of surface waters, in NK the presence of ice mélange prevented thermocline formation. In addition, a pronounced temperature minimum (~0 °C) at 10–20 m depth indicated the influence of subglacial discharge and upwelling (Mortensen et al., 2011). In both fjords, stratification also coincided with increased turbidity driven by suspended particulate matter from glacial runoff (Holding et al., 2019; Hopwood et al., 2018; Schlegel et al., 2024), which reduced light penetration and constrained photosynthesis (Meire et al., 2017). In NK, subglacial discharge also enhanced turbidity at depth. Nutrient dynamics showed a clear seasonal shift. Surface silicate concentrations were significantly higher than in spring, particularly in NK and inner AM, indicating substantial input from glacial meltwater and reduced biological uptake (Meire et al., 2016a). In contrast, nitrogen became the principal limiting nutrient (Fig. S6a). However, in NK, and especially the inner fjord, elevated NOx concentrations between 14-40 m indicated upwelling of nutrient-rich waters (Meire et al., 2017) which supported the development of a deep chlorophyll maximum. In AM, steep halo- and thermoclines combined with lower nitrogen availability compressed the productive layer to the surface. NH_4^+ concentrations were generally higher in summer compare to spring across both fjords, showing up-fjord gradients, especially between 10-40 m depth. In Kongsfjorden, Halbach et al. (Halbach et al., 2019) and van de Poll et al. (Van De Poll et al., 2016) reported elevated NH_4^+ concentrations mainly near the MTG, which they attributed to subglacial upwelling. The fact however that we observed similar (sub)surface NH_4^+ levels in both NK and AM, where no such upwelling is present, suggest that alternative sources such as enhanced microbial regeneration and zooplankton excretion may be involved. Despite these environmental differences, depth-integrated PP (0–50 m) during summer was relatively similar between the fjords, with values < ~500 mg C m^{-2} d^{-1}. In NK, PP decreased substantially relative to spring, particularly in the inner stations (e.g. GF12), likely due to increased turbidity and light limitation despite the presence of subsurface nutrients. In AM, PP was comparable to or only slightly lower than in spring. The lack of pronounced differences in PP between the MTG- and LTG-dominated fjords contrast with previous observations, which showed sustained higher PP during summer in NK (Meire et al., 2023). It is important to bear in mind however that our observations represent a temporal snapshot, and that productivity in Arctic fjords can vary rapidly in response to short-term changes in meltwater input, mixing intensity, and light availability.

The marked environmental differences between the fjords translated into a clear divergence in phytoplankton community structure. Phytoplankton communities in both fjords became dominated by pico- and nanophytoplankton, with diatom colonies being significantly less abundant and even nearly absent in AM. Here, strong stratification and limited nutrient supply led to a pronounced dominance of small green algae (*Ostreococcus, Micromonas, Bathycoccus, Pyramimonas*) and cryptophytes (*Teleaulax, Plagioselmis, Hemiselmis*), consistent with previous summer observations for this fjord (Stuart-Lee et al., 2023). Among Mamiellophyceae, *Micromonas* and *Bathycoccus* represent a typical component of summer Arctic picoplankton (Balzano et al., 2012; Lovejoy et al., 2007), including in fjord systems (Marquardt et al., 2016; Zhang et al., 2019). *Ostreococcus* has, to our knowledge, previously only been reported from Arctic waters in very low abundance (Belevich et al., 2021). Comparison of our *Ostreococcus* ASV with the Tara Oceans datasets (Vernette et al., 2021) revealed a 100 % sequence match to *Ostreococcus tauri* detected at two Tara stations (TARA_209 and TARA_196) in the SW Greenland region and the Beaufort Sea respectively, where it occurred in very low relative abundances (6.2×10^{-4} and 2.0×10^{-4}). Its consistent detection in our summer samples suggests that warmer and more nutrient-depleted surface conditions, as observed in the LTG fjord, may create favourable niches for this typically non-Arctic species at high latitudes. Cryptophytes are also a common component of Arctic summer

https://doi.org/10.5194/egusphere-2026-5308
Preprint. Discussion started: 11 September 2026

phytoplankton (Bae et al., 2022; Dąbrowska et al., 2021, 2025; Hegseth et al., 2019). Although microscopy-based studies in NK have not previously reported their presence, a recent analysis using flow cytometry detected summer concentrations up to 100 µg C L^{-1} in the same fjord (Rodríguez-Marconi et al., 2024), indicating that their abundance has been underestimated. Their prevalence in both fjords during summer is likely favoured by nutrient depletion, enhanced water column stratification, and surface freshening. Mixotrophy has been reported for some cryptophytes, particularly *Teleaulax* (Yoo et al., 2017), and may enhance competitiveness under nutrient limitation. In our dataset, *Teleaulax* also exhibited a clear negative relationship with salinity, consistent with findings from Adventfjorden (Svalbard) (Dąbrowska et al., 2021), indicating that lower salinity may favour the presence of specific cryptophyte taxa. The deeper waters of inner AM were also characterized by a relatively high contribution of the phagotrophic chrysophyte genus *Paraphysomonas* (Scoble and Cavalier-Smith, 2014). In Arctic environments—including Greenland—*Paraphysomonas* spp. have been reported from freshwater to marine systems, and some species are known to tolerate highly turbid conditions (D. Firsova et al., 2015; Kristiansen, 1992). The combination of low nutrient availability, elevated turbidity, and silica-rich conditions in inner AM may thus provide a favourable niche for this group, where reduced competition from siliceous phototrophs could further support its persistence. In NK, large nanophytoplankton dominated the assemblage. Metabarcoding and pigment ratios indicated that diatoms (*Chaetoceros*, *Thalassiosira*, and *Skeletonema*) were still a significant component of the phytoplankton. In mid-fjord stations, especially in NK, a large (> 300 µm) *Rhizosolenia* sp. was also important. Unfortunately, because cells were often broken, its contribution to total community biomass, which must be considerable given its size, could not be estimated. The persistent higher importance of diatoms in NK during summer is consistent with enhanced subsurface nutrient supply via subglacial discharge associated upwelling. Green algae and cryptophytes were also present in NK, although less than in AM. Pico- and smaller (2-5 µm) nanophytoplankton, which became more abundant in AM in summer (although their contribution to overall biomass was almost negligible), were positively correlated with NH_4^+, suggesting an enhanced capacity to exploit regenerated nitrogen sources, consistent with intensified microbial recycling in NO_x depleted, stratified surface waters. The overall shift towards nanophytoplankton during summer in both fjords may also be related to the higher availability of NH_4^+, as small phytoplankton are generally more reliant on NH_4^+ than larger diatoms (Probyn and Painting, 1985). In NK however, sustained NOx availability likely supported the persistence of diatoms, despite elevated NH_4^+ concentrations.

In summer, surface waters in outer NK were characterised by much higher nano- and microphytoplankton biomass compared to the rest of the fjord. Glacial meltwater enhances surface transport to the fjord mouth, which may promote the advection of phytoplankton to the outer sill region (GF3) (Mortensen et al., 2014). This accumulation, however, was not accompanied by elevated Chl a concentrations or higher PP. Imaging FCM revealed that cells in this region had on average lower autofluorescence signals (data not shown), suggesting that the elevated biomass in the outer fjord region likely reflected accumulation of less healthy or dying cells driven by estuarine circulation rather than *in situ* production.

Surface waters (1 m) in inner NK in contrast had very low phytoplankton biomass but were characterised by a unique community, dominated by the haptophyte *Pseudohaptolina*. Manual nBLAST of this ASV revealed a 100 % match (coverage and identity) (Sayers et al., 2025) with *P. sorokinii* (Orlova et al., 2016), currently recognised as *P. birgeri* (Ribeiro et al., 2020). This species was originally described from an exceptional under-ice bloom in coastal waters in the Sea of Japan, where it reached concentrations up to 7.4×10^7 cells L^{-1} (Orlova et al., 2016).

https://doi.org/10.5194/egusphere-2026-5308
Preprint. Discussion started: 11 September 2026

More recently, it has been classified as a harmful algal species in the North American Arctic–West Greenland region (Schiffrine et al., 2024), due to its capacity to form dense blooms that may affect local environment, highlighting the ecological relevance of this species at high latitudes. Given its association with ice-influenced environments, even transient occurrences may warrant attention in the context of future increases in meltwater-driven stratification.

5 Conclusion

Overall, this study highlights the central role of small phytoplankton in Greenland fjord ecosystems. While spring blooms were dominated by large chain-forming diatoms, summer communities shifted strongly towards pico- and, particularly, nano-sized phytoplankton, which represented an important component of total biomass and most likely also contributed substantially to primary production. This shift was especially pronounced under stratified, nutrient- and light-limited conditions, where small green algae, cryptophytes and other flagellates appeared favoured over large diatoms.

Our results also indicate that mixotrophy may be an important ecological strategy in Greenland fjords. The recurrent occurrence of taxa with known or potential mixotrophic capabilities suggests that flexible nutritional strategies may help to sustain microbial communities when inorganic nutrient availability and light conditions become limiting.

The detection of *Pseudohaptolina birgeri* in the ice-influenced surface waters of inner NK is particularly noteworthy. To our knowledge, this may represent the first report of this potentially harmful haptophyte from Greenland fjords. Its occurrence suggests that harmful or bloom-forming haptophytes may deserve greater attention in future monitoring of rapidly changing Arctic coastal systems.

Finally, this study also highlights important methodological limitations. Very large phytoplankton cells and colonies > 300 µm were not quantitatively included in our biomass estimates, meaning that the contribution of large diatoms such as *Rhizosolenia* to total biomass may have been underestimated. Future studies should combine high-throughput imaging and molecular approaches with traditional microscopic cell counts, focused on the larger microplankton, to better quantify large cells. Similarly, the contribution of dinoflagellates to primary production remains difficult to resolve, because metabarcoding does not allow a rigorous distinction between phototrophic, mixotrophic and heterotrophic taxa, while pigment-based approaches mainly capture peridinin-containing dinoflagellates. A more detailed assessment of dinoflagellate trophic strategies is therefore needed to better constrain their role in Arctic fjord productivity.

Data Availability

The dataset supporting this study has been deposited in the Zenodo repository (Mikhno et al., 2026). The high throughput sequence data have been deposited in the NCBI SRA under BioProject accession PRJNA1457328. Data are currently private and available to reviewers at:
https://dataview.ncbi.nlm.nih.gov/object/PRJNA1457328?reviewer=r877av930uvh65eq7fnri9rf3r
https://zenodo.org/records/20034759?preview=1&token=eyJhbGciOiJIUzUxMiJ9.eyJpZCI6IjI3Njg1Njc4LTk5ZWYtNDhhNC1hYzY0LWY1ZWI3ODM4ODQ2OSIsImRhdGEiOnt9LCJyYW5kb20iOiIxYjdkYzhjN2U2N2JmZTBkMzhmY2ViMDk5ZTg5ODgyNCJ9.3-a13rENliGXXI7ZUJiSqjMA9NdwDjz6eg1pGw6rL2ia9oqgHvR5y0LmgXwPHXSlvmtVnhvIaVarM5X4gI7M6A

https://doi.org/10.5194/egusphere-2026-5308
Preprint. Discussion started: 11 September 2026

Author contributions

MM: Conceptualization; Data curation; Formal analysis; Methodology; Writing – original draft; Writing – review & editing. LM: Funding acquisition; Methodology; Supervision; Writing – review & editing. RD: Methodology. PC: Methodology. ID: Methodology. SD: Methodology. KS: Conceptualization; Funding acquisition; Methodology; Project administration; Supervision; Writing – review & editing.

Competing interests

The authors declare that they have no conflict of interest.

Acknowledgements

We thank the captain of the RV *Avataq* for his invaluable assistance during fieldwork. We are also grateful to the staff of the Greenland Institute of Natural Resources (GINR) and to all collaborators in Greenland for their logistical and technical support during the sampling campaigns.

Financial support

This work is part of the IMAGIN project, funded by Research Foundation – Flanders (FWO) (grant no. 3G043120) and by the Belgian Federal Science Policy Office (BELSPO)-funded project CANOE (contract no. RV/21/CANOE). The research leading to the results presented in this publication was carried out with infrastructure funded by EMBRC Belgium – FWO international research infrastructures I001621N and I000825N.

https://doi.org/10.5194/egusphere-2026-5308
Preprint. Discussion started: 11 September 2026

References

Anderson, M. J. and Willis, T. J.: CANONICAL ANALYSIS OF PRINCIPAL COORDINATES: A USEFUL METHOD OF CONSTRAINED ORDINATION FOR ECOLOGY, Ecology, 84, 511–525, https://doi.org/10.1890/0012-9658(2003)084%5B0511:CAOPCA%5D2.0.CO;2, 2003.

Assmy, P., Cecilie Kvernvik, A., Hop, H., Hoppe, C. J. M., Chierici, M., David T., D., Duarte, P., Fransson, A., García, L. M., Patuła, W., Kwaśniewski, S., Maturilli, M., Pavlova, O., Tatarek, A., Wiktor, J. M., Wold, A., Wolf, K. K. E., and Bailey, A.: Seasonal plankton dynamics in Kongsfjorden during two years of contrasting environmental conditions, Progress in Oceanography, 213, 102996, https://doi.org/10.1016/j.pocean.2023.102996, 2023.

Bae, S., Kim, H., Nam, S.-I., Choi, K.-H., Kim, T.-W., Yun, S. T., Kim, H. S., Kim, T.-H., Han, D., Ko, Y. H., Kim, J.-H., Lim, Y. K., and Park, J. M.: The composition and abundance of phytoplankton after spring bloom in the Arctic Svalbard fjords, Estuarine, Coastal and Shelf Science, 275, 107970, https://doi.org/10.1016/j.ecss.2022.107970, 2022.

Balzano, S., Gourvil, P., Siano, R., Chanoine, M., Marie, D., Lessard, S., Sarno, D., and Vaulot, D.: Diversity of cultured photosynthetic flagellates in the North East Pacific and Arctic Oceans in summer, https://doi.org/10.5194/bgd-9-6219-2012, 1 June 2012., 2012.

Belevich, T. A., Milyutina, I. A., Abyzova, G. A., and Troitsky, A. V.: The pico-sized Mamiellophyceae and a novel *Bathycoccus* clade from the summer plankton of Russian Arctic Seas and adjacent waters, FEMS Microbiology Ecology, 97, fiaa251, https://doi.org/10.1093/femsec/fiaa251, 2021.

Blommaert, L., Huysman, M. J. J., Vyverman, W., Lavaud, J., and Sabbe, K.: Contrasting NPQ dynamics and xanthophyll cycling in a motile and a non-motile intertidal benthic diatom, Limnology & Oceanography, 62, 1466–1479, https://doi.org/10.1002/lno.10511, 2017.

Borcard, D., Gillet, F., and Legendre, P.: Numerical ecology with R, Second edition., Springer, Cham, 1 p., 2018.

Brzezinski, M. A.: THE Si:C:N RATIO OF MARINE DIATOMS: INTERSPECIFIC VARIABILITY AND THE EFFECT OF SOME ENVIRONMENTAL VARIABLES[1], Journal of Phycology, 21, 347–357, https://doi.org/10.1111/j.0022-3646.1985.00347.x, 1985.

Callahan, B. J., McMurdie, P. J., Rosen, M. J., Han, A. W., Johnson, A. J. A., and Holmes, S. P.: DADA2: High-resolution sample inference from Illumina amplicon data, Nat Methods, 13, 581–583, https://doi.org/10.1038/nmeth.3869, 2016.

Cape, M. R., Straneo, F., Beaird, N., Bundy, R. M., and Charette, M. A.: Nutrient release to oceans from buoyancy-driven upwelling at Greenland tidewater glaciers, Nature Geosci, 12, 34–39, https://doi.org/10.1038/s41561-018-0268-4, 2019.

Carr, J. R., Stokes, Chris. R., and Vieli, A.: Threefold increase in marine-terminating outlet glacier retreat rates across the Atlantic Arctic: 1992–2010, Ann. Glaciol., 58, 72–91, https://doi.org/10.1017/aog.2017.3, 2017.

Catlett, D. and Siegel, D. A.: Phytoplankton Pigment Communities Can be Modeled Using Unique Relationships With Spectral Absorption Signatures in a Dynamic Coastal Environment, JGR Oceans, 123, 246–264, https://doi.org/10.1002/2017JC013195, 2018.

Chitkara, C., Juul-Pedersen, T., Krawczyk, D., Søreide, J. E., Vader, A., Gradinger, R., Hs Winding, M., and Vonnahme, T. R.: Seasonality in phytoplankton communities and production in three Arctic fjords across a climate gradient, Progress in Oceanography, 227, 103317, https://doi.org/10.1016/j.pocean.2024.103317, 2024.

D. Firsova, A., Bessudova, A. Y., M. Sorokovikova, L., V. Tomberg, I., and V. Likhoshway, Y.: The Diversity of Chrysophycean Algae in an Arctic Zone of River and Sea Water Mixing, Russia, AJPS, 06, 2439–2452, https://doi.org/10.4236/ajps.2015.615246, 2015.

https://doi.org/10.5194/egusphere-2026-5308
Preprint. Discussion started: 11 September 2026

Dąbrowska, A. M., Wiktor, J. M., Wiktor, J. M., Kristiansen, S., Vader, A., and Gabrielsen, T.: When a Year Is Not Enough: Further Study of the Seasonality of Planktonic Protist Communities Structure in an Ice-Free High Arctic Fjord (Adventfjorden, West Spitsbergen), Water, 13, 1990, https://doi.org/10.3390/w13141990, 2021.

Dąbrowska, A. M., McGovern, M., Mazurkiewicz, M., and Poste, A.: Seasonal patterns and environmental drivers of protistan plankton along a terrestrial–marine gradient in Isfjorden (Svalbard), Front. Mar. Sci., 12, 1631963, https://doi.org/10.3389/fmars.2025.1631963, 2025.

Dvoretsky, A. G. and Dvoretsky, V. G.: Filling knowledge gaps in Arctic marine biodiversity: Environment, plankton, and benthos of Franz Josef Land, Barents Sea, Ocean & Coastal Management, 249, 106987, https://doi.org/10.1016/j.ocecoaman.2023.106987, 2024.

Egge, J. and Aksnes, D.: Silicate as regulating nutrient in phytoplankton competition, Mar. Ecol. Prog. Ser., 83, 281–289, https://doi.org/10.3354/meps083281, 1992.

Falkowski, P. G., Katz, M. E., Knoll, A. H., Quigg, A., Raven, J. A., Schofield, O., and Taylor, F. J. R.: The Evolution of Modern Eukaryotic Phytoplankton, Science, 305, 354–360, https://doi.org/10.1126/science.1095964, 2004.

Freyria, N. J., Joli, N., and Lovejoy, C.: A decadal perspective on north water microbial eukaryotes as Arctic Ocean sentinels, Sci Rep, 11, 8413, https://doi.org/10.1038/s41598-021-87906-4, 2021.

Graßhoff, K., Graßhoff, K., Kremling, K., and Ehrhardt, M. (Eds.): Methods of Seawater Analysis, 3. vollst. überarb. u. erw. Auflage., Wiley-VCH, Weinheim, 1 p., 2009.

Halbach, L., Vihtakari, M., Duarte, P., Everett, A., Granskog, M. A., Hop, H., Kauko, H. M., Kristiansen, S., Myhre, P. I., Pavlov, A. K., Pramanik, A., Tatarek, A., Torsvik, T., Wiktor, J. M., Wold, A., Wulff, A., Steen, H., and Assmy, P.: Tidewater Glaciers and Bedrock Characteristics Control the Phytoplankton Growth Environment in a Fjord in the Arctic, Front. Mar. Sci., 6, 254, https://doi.org/10.3389/fmars.2019.00254, 2019.

Han, D., Park, K.-T., Kim, H., Kim, T.-H., Jeong, M.-K., and Nam, S.-I.: Interaction between phytoplankton and heterotrophic bacteria in Arctic fjords during the glacial melting season as revealed by eDNA metabarcoding, FEMS Microbiology Ecology, 100, fiae059, https://doi.org/10.1093/femsec/fiae059, 2024.

Havskum, H. and Riemann, B.: Ecological importance of bacterivorous, pigmented flagellates (mixotrophs) in the Bay of Aarhus, Denmark, Mar. Ecol. Prog. Ser., 137, 251–263, https://doi.org/10.3354/meps137251, 1996.

Hegseth, E. N., Assmy, P., Wiktor, J. M., Wiktor, J., Kristiansen, S., Leu, E., Tverberg, V., Gabrielsen, T. M., Skogseth, R., and Cottier, F.: Phytoplankton Seasonal Dynamics in Kongsfjorden, Svalbard and the Adjacent Shelf, in: The Ecosystem of Kongsfjorden, Svalbard, vol. 2, edited by: Hop, H. and Wiencke, C., Springer International Publishing, Cham, 173–227, https://doi.org/10.1007/978-3-319-46425-1_6, 2019.

Hernando, M., Varela, D. E., Malanga, G., Almandoz, G. O., and Schloss, I. R.: Effects of climate-induced changes in temperature and salinity on phytoplankton physiology and stress responses in coastal Antarctica, Journal of Experimental Marine Biology and Ecology, 530–531, 151400, https://doi.org/10.1016/j.jembe.2020.151400, 2020.

Holding, J. M., Markager, S., Juul-Pedersen, T., Paulsen, M. L., Møller, E. F., Meire, L., and Sejr, M. K.: Seasonal and spatial patterns of primary production in a high-latitude fjord affected by Greenland Ice Sheet run-off, Biogeosciences, 16, 3777–3792, https://doi.org/10.5194/bg-16-3777-2019, 2019.

Hopwood, M. J., Carroll, D., Browning, T. J., Meire, L., Mortensen, J., Krisch, S., and Achterberg, E. P.: Non-linear response of summertime marine productivity to increased meltwater discharge around Greenland, Nat Commun, 9, 3256, https://doi.org/10.1038/s41467-018-05488-8, 2018.

Hopwood, M. J., Carroll, D., Dunse, T., Hodson, A., Holding, J. M., Iriarte, J. L., Ribeiro, S., Achterberg, E. P., Cantoni, C., Carlson, D. F., Chierici, M., Clarke, J. S., Cozzi, S., Fransson, A., Juul-Pedersen, T., Winding, M. H. S., and Meire, L.: Review article: How does glacier discharge affect marine biogeochemistry and primary production in the Arctic?, The Cryosphere, 14, 1347–1383, https://doi.org/10.5194/tc-14-1347-2020, 2020.

https://doi.org/10.5194/egusphere-2026-5308
Preprint. Discussion started: 11 September 2026

Jassby, A.: wql: Exploring Water Quality Monitoring Data, https://doi.org/10.32614/CRAN.package.wql, 2017.

Jefferis, G.: dendroextras: Extra Functions to Cut, Label and Colour Dendrogram Clusters, https://doi.org/10.32614/CRAN.package.dendroextras, 2013.

Jeffrey, S. W., Wright, S. W., and Zapata, M.: Microalgal classes and their signature pigments, in: Phytoplankton Pigments: Characterization, Chemotaxonomy and Applications in Oceanography, edited by: Roy, S., Llewellyn, C. A., Egeland, E. S., and Johnsen, G., Cambridge University Press, Cambridge, 3–77, https://doi.org/10.1017/CBO9780511732263.004, 2011.

Jimenez, V., Burns, J. A., Le Gall, F., Not, F., and Vaulot, D.: No evidence of Phago-mixotropy in *Micromonas polaris* (Mamiellophyceae), the Dominant Picophytoplankton Species in the Arctic, Journal of Phycology, 57, 435–446, https://doi.org/10.1111/jpy.13125, 2021.

Juul-Pedersen, T., Arendt, K., Mortensen, J., Blicher, M., Søgaard, D., and Rysgaard, S.: Seasonal and interannual phytoplankton production in a sub-Arctic tidewater outlet glacier fjord, SW Greenland, Mar. Ecol. Prog. Ser., 524, 27–38, https://doi.org/10.3354/meps11174, 2015.

Kanna, N., Sugiyama, S., Ando, T., Wang, Y., Sakuragi, Y., Hazumi, T., Matsuno, K., Yamaguchi, A., Nishioka, J., and Yamashita, Y.: Meltwater Discharge From Marine-Terminating Glaciers Drives Biogeochemical Conditions in a Greenlandic Fjord, Global Biogeochemical Cycles, 36, e2022GB007411, https://doi.org/10.1029/2022GB007411, 2022.

King, M. D., Howat, I. M., Jeong, S., Noh, M. J., Wouters, B., Noël, B., and Van Den Broeke, M. R.: Seasonal to decadal variability in ice discharge from the Greenland Ice Sheet, The Cryosphere, 12, 3813–3825, https://doi.org/10.5194/tc-12-3813-2018, 2018.

Kramer, S. J. and Siegel, D. A.: How Can Phytoplankton Pigments Be Best Used to Characterize Surface Ocean Phytoplankton Groups for Ocean Color Remote Sensing Algorithms?, JGR Oceans, 124, 7557–7574, https://doi.org/10.1029/2019JC015604, 2019.

Krawczyk, D. W., Witkowski, A., Juul-Pedersen, T., Arendt, K. E., Mortensen, J., and Rysgaard, S.: Microplankton succession in a SW Greenland tidewater glacial fjord influenced by coastal inflows and run-off from the Greenland Ice Sheet, Polar Biol, 38, 1515–1533, https://doi.org/10.1007/s00300-015-1715-y, 2015.

Krawczyk, D. W., Meire, L., Lopes, C., Juul-Pedersen, T., Mortensen, J., Li, C. L., and Krogh, T.: Seasonal succession, distribution, and diversity of planktonic protists in relation to hydrography of the Godthåbsfjord system (SW Greenland), Polar Biol, 41, 2033–2052, https://doi.org/10.1007/s00300-018-2343-0, 2018.

Kristiansen, J.: Silica-scaled chrysophytes from West Greenland: Disko Island and the Søndre Strømfjord region, Nordic Journal of Botany, 12, 525–536, https://doi.org/10.1111/j.1756-1051.1992.tb01831.x, 1992.

Latasa, M. and Bidigare, R. R.: A comparison of phytoplankton populations of the Arabian Sea during the Spring Intermonsoon and Southwest Monsoon of 1995 as described by HPLC-analyzed pigments, Deep Sea Research Part II: Topical Studies in Oceanography, 45, 2133–2170, https://doi.org/10.1016/S0967-0645(98)00066-6, 1998.

Legendre, P. and Legendre, L.: Numerical ecology, Third English edition., Elsevier, Amsterdam, 990 pp., 2012.

Lohr, M. and Wilhelm, C.: Xanthophyll synthesis in diatoms: quantification of putative intermediates and comparison of pigment conversion kinetics with rate constants derived from a model, Planta, 212, 382–391, https://doi.org/10.1007/s004250000403, 2001.

Lovejoy, C., Massana, R., and Pedrós-Alió, C.: Diversity and Distribution of Marine Microbial Eukaryotes in the Arctic Ocean and Adjacent Seas, Appl Environ Microbiol, 72, 3085–3095, https://doi.org/10.1128/AEM.72.5.3085-3095.2006, 2006.

Lovejoy, C., Vincent, W. F., Bonilla, S., Roy, S., Martineau, M., Terrado, R., Potvin, M., Massana, R., and Pedrós-Alió, C.: DISTRIBUTION, PHYLOGENY, AND GROWTH OF COLD-ADAPTED PICOPRASINOPHYTES IN ARCTIC SEAS[1], Journal of Phycology, 43, 78–89, https://doi.org/10.1111/j.1529-8817.2006.00310.x, 2007.

https://doi.org/10.5194/egusphere-2026-5308
Preprint. Discussion started: 11 September 2026

Lyngsgaard, M. M., Markager, S., and Richardson, K.: Changes in the vertical distribution of primary production in response to land-based nitrogen loading, Limnology & Oceanography, 59, 1679–1690, https://doi.org/10.4319/lo.2014.59.5.1679, 2014.

Marquardt, M., Vader, A., Stübner, E. I., Reigstad, M., and Gabrielsen, T. M.: Strong Seasonality of Marine Microbial Eukaryotes in a High-Arctic Fjord (Isfjorden, in West Spitsbergen, Norway), Appl Environ Microbiol, 82, 1868–1880, https://doi.org/10.1128/AEM.03208-15, 2016.

McKenrie, C. H., Deibel, D., Paranjape, M. A., and Thompson, R. J.: THE MARINE MIXOTROPH *DINOBRYON BALTICUM* (CHRYSOPHYCEAE): PHAGOTROPHY AND SURVIVAL IN A COLD OCEAN[1], Journal of Phycology, 31, 19–24, https://doi.org/10.1111/j.0022-3646.1995.00019.x, 1995.

McKie-Krisberg, Z. M. and Sanders, R. W.: Phagotrophy by the picoeukaryotic green alga *Micromonas* : implications for Arctic Oceans, The ISME Journal, 8, 1953–1961, https://doi.org/10.1038/ismej.2014.16, 2014.

McKie-Krisberg, Z. M., Sanders, R. W., and Gast, R. J.: Evaluation of Mixotrophy-Associated Gene Expression in Two Species of Polar Marine Algae, Front. Mar. Sci., 5, 273, https://doi.org/10.3389/fmars.2018.00273, 2018.

McMurdie, P. J. and Holmes, S.: phyloseq: An R Package for Reproducible Interactive Analysis and Graphics of Microbiome Census Data, PLoS ONE, 8, e61217, https://doi.org/10.1371/journal.pone.0061217, 2013.

Meire, L., Søgaard, D. H., Mortensen, J., Meysman, F. J. R., Soetaert, K., Arendt, K. E., Juul-Pedersen, T., Blicher, M. E., and Rysgaard, S.: Glacial meltwater and primary production are drivers of strong CO_2 uptake in fjord and coastal waters adjacent to the Greenland Ice Sheet, Biogeosciences, 12, 2347–2363, https://doi.org/10.5194/bg-12-2347-2015, 2015.

Meire, L., Meire, P., Struyf, E., Krawczyk, D. W., Arendt, K. E., Yde, J. C., Juul Pedersen, T., Hopwood, M. J., Rysgaard, S., and Meysman, F. J. R.: High export of dissolved silica from the Greenland Ice Sheet, Geophysical Research Letters, 43, 9173–9182, https://doi.org/10.1002/2016GL070191, 2016a.

Meire, L., Mortensen, J., Rysgaard, S., Bendtsen, J., Boone, W., Meire, P., and Meysman, F. J. R.: Spring bloom dynamics in a subarctic fjord influenced by tidewater outlet glaciers (Godthåbsfjord, SW Greenland), JGR Biogeosciences, 121, 1581–1592, https://doi.org/10.1002/2015JG003240, 2016b.

Meire, L., Mortensen, J., Meire, P., Juul-Pedersen, T., Sejr, M. K., Rysgaard, S., Nygaard, R., Huybrechts, P., and Meysman, F. J. R.: Marine-terminating glaciers sustain high productivity in Greenland fjords, Global Change Biology, 23, 5344–5357, https://doi.org/10.1111/gcb.13801, 2017.

Meire, L., Paulsen, M. L., Meire, P., Rysgaard, S., Hopwood, M. J., Sejr, M. K., Stuart-Lee, A., Sabbe, K., Stock, W., and Mortensen, J.: Glacier retreat alters downstream fjord ecosystem structure and function in Greenland, Nat. Geosci., 16, 671–674, https://doi.org/10.1038/s41561-023-01218-y, 2023.

Menden-Deuer, S. and Lessard, E. J.: Carbon to volume relationships for dinoflagellates, diatoms, and other protist plankton, Limnology & Oceanography, 45, 569–579, https://doi.org/10.4319/lo.2000.45.3.0569, 2000.

Mikhno, M., Dasseville, R., Chaerle, P., Ilse, D., D'hondt, S., Meire, L., and Sabbe, K.: Seasonal divergence in phytoplankton community and size structure between contrasting fjord types in SW Greenland, https://doi.org/10.5281/ZENODO.20034759, 2026.

Mortensen, J., Lennert, K., Bendtsen, J., and Rysgaard, S.: Heat sources for glacial melt in a sub-Arctic fjord (Godthåbsfjord) in contact with the Greenland Ice Sheet, J. Geophys. Res., 116, C01013, https://doi.org/10.1029/2010JC006528, 2011.

Mortensen, J., Bendtsen, J., Motyka, R. J., Lennert, K., Truffer, M., Fahnestock, M., and Rysgaard, S.: On the seasonal freshwater stratification in the proximity of fast-flowing tidewater outlet glaciers in a sub-Arctic sill fjord, JGR Oceans, 118, 1382–1395, https://doi.org/10.1002/jgrc.20134, 2013.

Mortensen, J., Bendtsen, J., Lennert, K., and Rysgaard, S.: Seasonal variability of the circulation system in a west Greenland tidewater outlet glacier fjord, Godthåbsfjord (64°N): Godthåbsfjord, J. Geophys. Res. Earth Surf., 119, 2591–2603, https://doi.org/10.1002/2014JF003267, 2014.

https://doi.org/10.5194/egusphere-2026-5308
Preprint. Discussion started: 11 September 2026

Nielsen, E. S.: The Use of Radio-active Carbon (C14) for Measuring Organic Production in the Sea, ICES Journal of Marine Science, 18, 117–140, https://doi.org/10.1093/icesjms/18.2.117, 1952.

Oksanen, J., Simpson, G. L., Blanchet, F. G., Kindt, R., Legendre, P., Minchin, P. R., O'Hara, R. B., Solymos, P., Stevens, M. H. H., Szoecs, E., Wagner, H., Bedward, M., Bolker, B., Borcard, D., Carvalho, G., De Caceres, M., Durand, S., Evangelista, H. B. A., Hannigan, G., Hill, M. O., Lahti, L., Martino, C., Ouellette, M.-H., Ribeiro Cunha, E., Smith, T., Stier, A., Ter Braak, C. J. F., and Weedon, J.: vegan: Community Ecology Package, https://doi.org/10.32614/CRAN.package.vegan, 2025.

Orlova, T. Yu., Efimova, K. V., and Stonik, I. V.: Morphology and molecular phylogeny of *Pseudohaptolina sorokinii sp. nov* . (Prymnesiales, Haptophyta) from the Sea of Japan, Russia, Phycologia, 55, 506–514, https://doi.org/10.2216/15-107.1, 2016.

Peperzak, L., Colijn, F., Gieskes, W. W. C., and Peeters, J. C. H.: Development of the diatom- *Phaeocystis* spring bloom in the Dutch coastal zone of the North Sea: the silicon depletion versus the daily irradiance threshold hypothesis, J Plankton Res, 20, 517–537, https://doi.org/10.1093/plankt/20.3.517, 1998.

Probyn, T. A. and Painting, S. J.: Nitrogen uptake by size-fractionated phytoplankton populations in Antarctic surface waters1, Limnology & Oceanography, 30, 1327–1332, https://doi.org/10.4319/lo.1985.30.6.1327, 1985.

R Core Team: R: A Language and Environment for Statistical Computing, 2021.

Redfield, A. C.: On the proportions of organic derivatives in sea water and their relation to the composition of plankton., University Press of Liverpool, 177−192, 1934.

Redfield, A. C.: The biological control of chemical factors in the environment., 46, 205−221, 1958.

Ribeiro, C. G., Dos Santos, A. L., Probert, I., Vaulot, D., and Edvardsen, B.: Taxonomic reassignment of *Pseudohaptolina birgeri comb. nov* . (Haptophyta), Phycologia, 59, 606–615, https://doi.org/10.1080/00318884.2020.1830255, 2020.

Rodríguez-Marconi, S., Krock, B., Tillmann, U., Tillmann, A., Voss, D., Zielinski, O., Vásquez, M., and Trefault, N.: Diversity of eukaryote plankton and phycotoxins along the West Kalaallit Nunaat (Greenland) coast, Front. Mar. Sci., 11, 1443389, https://doi.org/10.3389/fmars.2024.1443389, 2024.

Rysgaard, S., Mortensen, J., Juul-Pedersen, T., Sørensen, L. L., Lennert, K., Søgaard, D. H., Arendt, K. E., Blicher, M. E., Sejr, M. K., and Bendtsen, J.: High air–sea CO2 uptake rates in nearshore and shelf areas of Southern Greenland: Temporal and spatial variability, Marine Chemistry, 128–129, 26–33, https://doi.org/10.1016/j.marchem.2011.11.002, 2012.

Rytter Hasle, G. and Riddervold Heimdal, B.: The net phytoplankton in Kongsfjorden, Svalbard, July 1988, with general remarks on species composition of Arctic phytoplankton, Polar Research, 17, 31–52, https://doi.org/10.3402/polar.v17i1.6605, 1998.

Sayers, E. W., Beck, J., Bolton, E. E., Brister, J. R., Chan, J., Connor, R., Feldgarden, M., Fine, A. M., Funk, K., Hoffman, J., Kannan, S., Kelly, C., Klimke, W., Kim, S., Lathrop, S., Marchler-Bauer, A., Murphy, T. D., O'Sullivan, C., Schmieder, E., Skripchenko, Y., Stine, A., Thibaud-Nissen, F., Wang, J., Ye, J., Zellers, E., Schneider, V. A., and Pruitt, K. D.: Database resources of the National Center for Biotechnology Information in 2025, Nucleic Acids Research, 53, D20–D29, https://doi.org/10.1093/nar/gkae979, 2025.

Schiffrine, N., Dhifallah, F., Dionne, K., Poulin, M., Lessard, S., Rochon, A., and Gosselin, M.: Microbial plankton occurrence database in the North American Arctic region: synthesis of recent diversity of potentially toxic and/or harmful algae, Earth Syst. Sci. Data, 16, 5681–5701, https://doi.org/10.5194/essd-16-5681-2024, 2024.

Schlegel, R. W., Singh, R. K., Gentili, B., Bélanger, S., Castro De La Guardia, L., Krause-Jensen, D., Miller, C. A., Sejr, M., and Gattuso, J.-P.: Underwater light environment in Arctic fjords, Earth Syst. Sci. Data, 16, 2773–2788, https://doi.org/10.5194/essd-16-2773-2024, 2024.

https://doi.org/10.5194/egusphere-2026-5308
Preprint. Discussion started: 11 September 2026

Schneider, C. A., Rasband, W. S., and Eliceiri, K. W.: NIH Image to ImageJ: 25 years of image analysis, Nat Methods, 9, 671–675, https://doi.org/10.1038/nmeth.2089, 2012.

Scoble, J. M. and Cavalier-Smith, T.: Scale evolution in Paraphysomonadida (Chrysophyceae): Sequence phylogeny and revised taxonomy of Paraphysomonas, new genus Clathromonas, and 25 new species, European Journal of Protistology, 50, 551–592, https://doi.org/10.1016/j.ejop.2014.08.001, 2014.

Seelam, J. S., Fernandes De Souza, M., Chaerle, P., Willems, B., Michels, E., Vyverman, W., and Meers, E.: Maximizing nutrient recycling from digestate for production of protein-rich microalgae for animal feed application, Chemosphere, 290, 133180, https://doi.org/10.1016/j.chemosphere.2021.133180, 2022.

Sekiguchi, H., Kawachi, M., Nakayama, T., and Inouye, I.: A taxonomic re-evaluation of the Pedinellales (Dictyochophyceae), based on morphological, behavioural and molecular data, Phycologia, 42, 165–182, https://doi.org/10.2216/i0031-8884-42-2-165.1, 2003.

Sieracki, C., Sieracki, M., and Yentsch, C.: An imaging-in-flow system for automated analysis of marine microplankton, Mar. Ecol. Prog. Ser., 168, 285–296, https://doi.org/10.3354/meps168285, 1998.

Smith, W. O. and Trimborn, S.: *Phaeocystis* : A Global Enigma, Annu. Rev. Mar. Sci., 16, 417–441, https://doi.org/10.1146/annurev-marine-022223-025031, 2024.

Stoeck, T., Bass, D., Nebel, M., Christen, R., Jones, M. D. M., Breiner, H., and Richards, T. A.: Multiple marker parallel tag environmental DNA sequencing reveals a highly complex eukaryotic community in marine anoxic water, Molecular Ecology, 19, 21–31, https://doi.org/10.1111/j.1365-294X.2009.04480.x, 2010.

Stoecker, D. K. and Lavrentyev, P. J.: Mixotrophic Plankton in the Polar Seas: A Pan-Arctic Review, Front. Mar. Sci., 5, 292, https://doi.org/10.3389/fmars.2018.00292, 2018.

Stuart-Lee, A. E., Mortensen, J., Kaaden, A. -S. V. D., and Meire, L.: Seasonal Hydrography of Ameralik: A Southwest Greenland Fjord Impacted by a Land-Terminating Glacier, JGR Oceans, 126, e2021JC017552, https://doi.org/10.1029/2021JC017552, 2021.

Stuart-Lee, A. E., Mortensen, J., Juul-Pedersen, T., Middelburg, J. J., Soetaert, K., Hopwood, M. J., Engel, A., and Meire, L.: Influence of glacier type on bloom phenology in two Southwest Greenland fjords, Estuarine, Coastal and Shelf Science, 284, 108271, https://doi.org/10.1016/j.ecss.2023.108271, 2023.

The IMBIE Team: Mass balance of the Greenland Ice Sheet from 1992 to 2018, Nature, 579, 233–239, https://doi.org/10.1038/s41586-019-1855-2, 2020.

Van De Poll, W. H., Maat, D. S., Fischer, P., Rozema, P. D., Daly, O. B., Koppelle, S., Visser, R. J. W., and Buma, A. G. J.: Atlantic Advection Driven Changes in Glacial Meltwater: Effects on Phytoplankton Chlorophyll-a and Taxonomic Composition in Kongsfjorden, Spitsbergen, Front. Mar. Sci., 3, https://doi.org/10.3389/fmars.2016.00200, 2016.

Van Den Broeke, M. R., Enderlin, E. M., Howat, I. M., Kuipers Munneke, P., Noël, B. P. Y., Van De Berg, W. J., Van Meijgaard, E., and Wouters, B.: On the recent contribution of the Greenland ice sheet to sea level change, The Cryosphere, 10, 1933–1946, https://doi.org/10.5194/tc-10-1933-2016, 2016.

Van Heukelem, L. and Thomas, C. S.: Computer-assisted high-performance liquid chromatography method development with applications to the isolation and analysis of phytoplankton pigments, Journal of Chromatography A, 910, 31–49, https://doi.org/10.1016/S0378-4347(00)00603-4, 2001.

Vaulot, D., Campo, J. D., Mahwash Jamy, Burki, F., Guillou, L., Santoferrara, L., Ganser, M., De Oliveira Da Rocha Franco, A., Mertens, K., Haifeng Gu, Jang, S. H., Škaloud, P., Dünn, M., Gross, M., Алексей Селюк, Sandin, M. M., Metz, S., Dorrell, R., and AnnaMaria Fiore-Donno: pr2database/pr2database: PR2 version 5.0.0 (v5.0.0), https://doi.org/10.5281/ZENODO.7805244, 2023.

Vernette, C., Henry, N., Lecubin, J., De Vargas, C., Hingamp, P., and Lescot, M.: The Ocean barcode atlas: A web service to explore the biodiversity and biogeography of marine organisms, Molecular Ecology Resources, 21, 1347–1358, https://doi.org/10.1111/1755-0998.13322, 2021.

https://doi.org/10.5194/egusphere-2026-5308
Preprint. Discussion started: 11 September 2026

Vidussi, F., Claustre, H., Manca, B. B., Luchetta, A., and Marty, J.: Phytoplankton pigment distribution in relation to upper thermocline circulation in the eastern Mediterranean Sea during winter, J. Geophys. Res., 106, 19939–19956, https://doi.org/10.1029/1999JC000308, 2001.

White, P. L., Bertrand, E. M., Spence, J. S., Cavaco, M. A., Parrott, C., Waterman, S., Rowland, E., Roberts, M. E., Noah, T., Mellett, T., Hallé, D., Hamilton, A. K., Bundy, R. M., Didier, D., and Bhatia, M. P.: Shifting phytoplankton ecological strategies along a continuum of tidewater glacier retreat, ISME Communications, 5, ycaf045, https://doi.org/10.1093/ismeco/ycaf045, 2025.

Wickham, H.: ggplot2, Springer International Publishing, Cham, https://doi.org/10.1007/978-3-319-24277-4, 2016.

Yoo, Y. D., Seong, K. A., Jeong, H. J., Yih, W., Rho, J.-R., Nam, S. W., and Kim, H. S.: Mixotrophy in the marine red-tide cryptophyte Teleaulax amphioxeia and ingestion and grazing impact of cryptophytes on natural populations of bacteria in Korean coastal waters, Harmful Algae, 68, 105–117, https://doi.org/10.1016/j.hal.2017.07.012, 2017.

Zhang, F., Cao, S., Gao, Y., and He, J.: Distribution and environmental correlations of picoeukaryotes in an Arctic fjord (Kongsfjorden, Svalbard) during the summer, Polar Research, 38, https://doi.org/10.33265/polar.v38.3390, 2019.